Drastic changes in the distribution of branched tetraether lipids in suspended matter and sediments from the Yenisei River and Kara Sea (Siberia): Implications for the use of brGDGT-based proxies in coastal marine sediments

Cindy De Jonge[a*], Alina Stadnitskaia[a], Ellen C. Hopmans[a], Georgy Cherkashov[b], Andrey Fedotov[c], Irina D. Streletskaya[d], Alexander A. Vasiliev[e] and Jaap S. Sinninghe Damsté[a]

[a] Department of Marine Organic Biogeochemistry, NIOZ Royal Netherlands Institute for Sea Research, P.O. Box 59, 1790 AB Den Burg (Texel), The Netherlands

[b] All-Russian Research Institute for Geology and Mineral Resources of the World Ocean (VNIIOkeangeologia), Ministry of Natural Resources, Russian Academy of Science, St. Petersburg, Russian Federation

[c] Limnological Institute, Siberian Branch of the Russian Academy of Sciences, Irkutsk, Russian Federation

[d] Moscow MV Lomonosov State University, Department of Geography, Moscow, Russian Federation

[e] Siberian Branch, Russian Academy of Sciences, Earth Cryosphere Institute, Tumen, Russian Federation

* Corresponding author.

E-mail address: dejonge.cindy@gmail.com

ABSTRACT

The distribution of branched glycerol dialkyl glycerol tetraethers (brGDGTs) in soils has been shown to correlate with pH and mean annual air temperature. Because of this dependence brGDGTs have found an application as palaeoclimate proxies in coastal marine sediments, based on the assumption that their distribution is not altered during the transport from soils to marine systems by rivers. To study the processes acting on the brGDGT distributions, we analysed the full suite of brGDGTs, including the recently described 6-Me brGDGTs, in both the suspended particulate matter (SPM) of the Siberian Yenisei River and the SPM and sediments of its outflow in the Kara Sea. The brGDGT distribution in the SPM of the Yenisei River was fairly constant and characterized by high abundances of the 6-Me brGDGTs, reflecting their production at the neutral pH of the river water. However, the brGDGT distribution showed marked shifts in the marine system. Firstly, in the Yenisei River Mouth, the fractional abundance of the 6-Me brGDGTs decreases sharply. The brGDGT signature in the Yenisei River Mouth possibly reflects brGDGTs delivered during the spring floods that may carry a different distribution. Also, coastal cliffs were shown to contain brGDGTs and to influence especially those sites without major river inputs (e.g. Khalmyer Bay). Further removed from the river mouth, in-situ production of brGDGTs in the marine system influences the distribution. However, also the fractional abundance of the tetramethylated brGDGT Ia increases, resulting in a distribution that is distinct from in-situ produced signals at similar latitudes (Svalbard). We suggest that this shift may be caused by preferential degradation of labile (riverine in-situ produced) brGDGTs and the subsequent enrichment in less labile (soil) material. The offshore distribution indeed agrees with the brGDGT distribution encountered in a lowland peat. This implies that the offshore Kara Sea sediments possibly carry a soil-dominated signal, indicating potential for palaeoclimate reconstructions at this site.

Both in the river system and coastal cliffs, brGDGTs were much more abundant than crenarchaeol, an archaeal isoprenoid GDGT, resulting in high (>0.93) Branched and Isoprenoid Tetraether (BIT) index values. Moving downstream in the marine sediments, a decrease in brGDGT concentrations, coeval with an increase in crenarchaeol, resulted in decreasing BIT index values. This decrease correlates with changes in bulk proxies for terrigenous input ($\delta^{13}C_{org}$, C/N), confirming the

use of the BIT index to trace the delivery of river-transported and coastal cliff-derived terrigenous organic matter.

Keywords

Branched GDGT, riverine and marine SPM, marine sediments, in-situ production, preferential degradation, Kara Sea.

1. Introduction

Branched glycerol dialkyl glycerol tetraethers (brGDGTs) are bacterial membrane lipids (Weijers et al., 2006; Sinninghe Damsté et al., 2011) that are ubiquitous in soils and peat (e.g. Weijers et al. 2007a, Weijers et al., 2009). They are also found in marine river fan sediments, deposited by rivers after erosion and transport of soil particles (Hopmans et al., 2004). The amount of terrigenous brGDGTs relative to the amount of crenarchaeol, a marine Thaumarchaeotal isoprenoid GDGT (Sinninghe Damsté et al., 2002), can be expressed in the Branched Isoprenoid Tetraether (BIT) index (Hopmans et al., 2004). The BIT index has been used to trace the input of soil-derived organic matter from river systems to the marine environment in polar (Doğrul Selver at al., 2015; Sparkes et al., 2015), temperate (e.g. Kim et al., 2006; Zell et al., 2014a) and tropical (e.g. Zell et al., 2014b) climate zones. BrGDGTs also find an application in palaeoclimate reconstructions. They possess 4 to 6 methyl substituents ('branches') on the linear C_{28} alkyl chains and up to two cyclopentyl moieties formed by internal cyclization (Fig. 1; Schouten et al., 2000; Sinninghe Damsté et al., 2000; Weijers et al., 2006). In a dataset of global soils, the structural diversity of nine brGDGTs was shown to correlate with the prevailing soil pH and the mean annual air temperature (MAT) (Weijers et al., 2007a). The Cyclization of Branched Tetraethers (CBT) and the Methylation of Branched Tetraethers (MBT) are two brGDGT indices that have been successfully applied to reconstruct the palaeoclimate in a variety of settings; palaeosoils (e.g. Peterse et al., 2011, 2014a, Gao et al., 2012), speleothems (e.g. Yang et al., 2011), lake sediments (e.g. Tyler et al., 2010; Niemann et al., 2012) but firstly in marine sediments. In the Congo River fan, brGDGTs have been used to reconstruct continental palaeoclimate changes over the past 25 kyr B.P. (Weijers et al., 2007b), and in the Amazon River fan sediments palaeoclimatic changes since 37 kyr B.P. were reconstructed (Bendle et al., 2010). Older samples allowed the reconstruction of the temperature changes in the Arctic during the Paleocene-Eocene (Weijers et al., 2007c) and Eocene-Oligocene boundary (Schouten et al., 2008). Donders et al. (2009) reconstructed a cooling trend in Miocene Northern Europe, while Pross et al. (2012) used CBT/MBT to reconstruct temperatures along the Atlantic coast during the early Eocene.

These previous studies have all been based on the assumption that the majority of the brGDGTs encountered in marine sediments are derived from soils. However, in-situ production of

63 brGDGTs has been shown to occur in lakes (e.g. Sinninghe Damsté et al., 2009; Loomis et al., 2011,
64 2014). This process was also demonstrated in rivers: by Tierney and Russell (2009) in a set of small
65 African rivers, by Kim et al. (2012) and Zell et al. (2013) in the Amazon River, by Zhang et al. (2012)
66 and Yang et al. (2013) in the Chinese Yangtze River, by De Jonge et al. (2014a) in the Siberian Yenisei
67 River and by Zell et al. (2014a) in the Portuguese Tagus River. These studies showed that an aquatic
68 in-situ produced signal can influence or even dominate the brGDGT distribution delivered by the
69 surrounding watershed. This possibly complicates palaeoclimate reconstructions.

70 In-situ production of brGDGTs in the marine system may also influence brGDGT
71 distributions. This was shown by a number of recent studies that compare the brGDGT signature of
72 recent sediments and/or suspended particulate matter (SPM) with continental and/or riverine material
73 in coastal marine settings. Peterse et al. (2009) made a comparison of the brGDGTs downstream a
74 high latitude fjord (Svalbard, Norway). They showed that an increase in the amount of brGDGTs
75 downstream and an increased fractional abundance of the cyclopentane-containing brGDGT in the
76 marine sediments are indicative of in-situ production of brGDGTs. Zhu et al. (2011) also observed an
77 increase in the brGDGT concentration offshore the Chinese Yangtze River and an increase in the
78 cyclopentane-containing brGDGTs Ic and IIc, concluding that significant in-situ production is likely.
79 Zell et al. (2014b) observed a strong decrease in the fractional abundance of brGDGT Ia in the marine
80 sediments that were not influenced by the Amazon River plume, coeval with an increase of the
81 cyclopentane-containing brGDGTs. They invoked in-situ production of brGDGTs in the marine
82 sediments to explain the results from Bendle et al. (2010), who reconstructed unexpected temperature
83 shifts based on the brGDGT distribution in the Amazon River fan sediments. A study of the brGDGT
84 distribution in the Tagus basin and its outflow in the marine system also indicated an increase in the
85 fractional abundance of cyclopentane-containing brGDGTs (Zell et al., 2014a).

86 All studies referred to above employed an HPLC-based chromatographic method, as described
87 by Schouten et al. (2007), that allowed quantification of nine individual brGDGTs (Fig. 1). However,
88 using this chromatographic method, a set of novel brGDGT components recently described by De
89 Jonge et al. (2013), is not separated. These components were shown to possess a methyl group at the 6
90 and/or ω6 position, rather than at the 5 and/or ω5 position, as had been described previously for

91 brGDGT IIa and IIIa by Sinninghe Damsté et al. (2000). De Jonge et al. (2013) showed that in a
92 Siberian peat both the pentamethylated and hexamethylated (non-cyclopentane containing) brGDGTs
93 exist as a 5- and 6-Me component (respectively IIa and IIa' and IIIa and IIIa'; Fig. 1). With the
94 application of a silica HPLC column, De Jonge et al. (2014a) were able to show that the
95 hexamethylated 6-Me brGDGTs were abundant in the Yenisei River SPM, and probably also occurred
96 with one or two cyclopentane groups. Application of a further improved HPLC method on a set of
97 global soils allowed quantification of six penta- and hexamethylated 6-Me brGDGTs (De Jonge et al.,
98 2014b) and revealed that the 6-Me brGDGTs are abundant, comprising on average 24% of the total
99 amount of brGDGTs. Evaluating the influence of the 6-Me brGDGTs on the existing CBT and MBT'-
100 proxies shows that exclusion of the 6-Me brGDGTs results in an index (the MBT'_{5ME}) that shows an
101 improved correlation with MAT and is no longer dependent on pH. In contrast to the findings by
102 Weijers et al. (2007a) and Peterse et al. (2012), a first-order correlation between the MBT'_{5ME} and the
103 MAT is now possible. De Jonge et al. (2014b) also showed that a novel brGDGT index (CBT') and a
104 multiple linear regression of the fractional abundances of the brGDGTs (MAT_{mr}), further improved the
105 accuracy of the reconstructed pH and MAT, respectively.
106 This study describes for the first time the abundance of both the 5- and 6-Me brGDGTs in a
107 dataset of riverine and marine SPM and sediments. We compare the brGDGT distribution delivered by
108 the river with the signal encountered in the marine sediments, and evaluate the changes in brGDGT
109 distributions. We also evaluate the performance of the BIT-index in the Yenisei River outflow,
110 comparing it with bulk organic matter properties ($\delta^{13}C_{org}$, C/N). To evaluate the extent to which the
111 observed changes in brGDGT distributions can affect palaeoclimate reconstructions, we calculate the
112 reconstructed pH and MAT using the novel CBT' and MAT_{mr} (De Jonge et al., 2014b).
113
114 **2. Study area**
115 The Kara Sea is the second largest shelf area of the Arctic Ocean, partially enclosed to the
116 west by the Novaya Zemblya and Franz Josef Land, to the south by the Siberian mainland and to the
117 east by the Zevernaya Archipelago and the Taimyr Peninsula. To the north, the Kara Sea shelf is open
118 to the Arctic Ocean (Fig. 2A). About one third of the total freshwater discharge into the Arctic Ocean

occurs through river run-off (Aagaard and Coachman, 1975). A fifth of the continental run-off of the Eurasian continent drains into the Kara Sea (Lammers et al., 2001). The resulting water discharges of the Ob and Yenisei River reach 400 and 630 km^3/year, ranking them thirteenth and sixth in the world in terms of water discharge (Bobrovitskaya et al., 1996). The Ob and Yenisei River estuaries are separated by the Gydan Peninsula, where the narrow and deep Khalmyer Bay is situated. North of its shore are a number of islands; the Oleniy and Sibiriakov Islands (Fig. 2A).

The Yenisei discharge and Kara Sea circulation are characterized by a strong seasonality. During the summer months, the surface currents in the Kara Sea follow a cyclonic circulation. The Greenland current enters the Kara Sea from the north, and passes along the east coast of Novaya Zemlya. This water body is then joined by the discharge of the Ob and Yenisei Rivers, before flowing further to the northeast (e.g. Lisitsyn, 1995; Pavlov and Pfirman, 1995). From mid-October to mid-May, when only 10-15% of the river discharge happens (e.g. Pavlov and Pfirman, 1995), the Kara Sea and Yenisei River estuary are almost entirely ice-covered. The ice preserves the uppermost water layers against wind mixing, and therefore the freshwater layer extends for a large distance under the ice, dispersing the little material delivered over a large distance (Lisitsyn, 1995). Between June and September, when most of the discharge happens (ca. 80%, e.g. Pavlov and Pfirman, 1995), the bulk of suspended load is deposited in front of the estuaries (Lisitsyn, 1995). Between the surface isohaline of 2 and 20 psu, concentrations of suspended load decrease with an order of magnitude compared to the estuary (Lisitsyn, 1995). The high discharge period is characterized by a strong thermal stratification. Below the warm, fresh surface water, a salt-water tongue is present at 6-8 m in the inner Kara Sea, flowing onshore (Pavlov and Pfirman, 1995). Present sedimentation rates in the southern Kara Sea are estimated to range between approximately 0.2 to 1 mm/yr, with the exception of shallow areas that are subjected to winnowing (e.g. Polyak et al., 2000). Sedimentation fluxes are highest in autumn and during the ice-covered months (Gaye et al., 2007).

147 **3. Material and methods**

148 *3.1. Collection of samples.*

149 Table 1 lists the SPM and sediment samples investigated in this study and the location of the
150 sampling stations are shown in Fig. 2. In August-September 2009, surface water (<10 m depth; 1-300
151 L) was collected and filtered at 30 locations distributed throughout the Kara Sea and at 9 locations
152 along the Yenisei River, from the R/V Sovetskaya Arktika. At 15 sites, surface sediment samples were
153 obtained by gravity coring. In September 2011, SPM (120-150 L) and surface sediments (obtained by
154 box cores) were sampled at nine sites throughout the Kara Sea, from the R/V Akademik Mstislav
155 Keldysh. The SPM from both the 2009 and 2011 expeditions was collected with an in-situ pump
156 (McLane Large Volume Water Transfer System Sampler), on 0.7 μm pore size GF/F glass fiber filters.
157 In July 2010, three SPM samples were obtained in tributaries of the Angara River and in the Selenga
158 River. Surface water was collected in canisters after wading several meters into the river and filtered
159 using the same filters, a peristaltic pump and a titanium tripod system. Care was taken to sample
160 flowing water in the river, avoiding zones with stagnant water. One surface peat sample was collected
161 in the floodplain of a lake. The TOC-normalized concentrations of the GDGTs in the Yenisei River
162 SPM have been previously reported in De Jonge et al. (2014a). The values reported here are obtained
163 independently, after extraction of the remaining half of the filters. In 2009, coastal cliffs were sampled
164 at five sites, after removal of the exposed layer. The samples were taken on the east bank on the
165 Yenisei River Mouth and Gulf, with one sample taken on Sibiriakov Island. Furthermore, a lowland
166 peat that overlies a buried glacier was sampled in an outcrop, 1.95 m below the surface.

167

168 *3.2. Lipid extraction and GDGT analyses.*

169 Freeze-dried filters, sediments, coastal cliffs and soils (0.5-5 g) were extracted using a modified
170 Bligh and Dyer method as described by Pitcher et al. (2009). The samples were ultrasonically
171 extracted three times for 10 min using a single-phase solvent mixture of MeOH/DCM/phosphate
172 buffer 10:5:4 (v/v/v). The extract was separated into a core lipid (CL) and intact polar lipid (IPL)
173 fraction over a small silica column, using a procedure modified from Pitcher et al. (2009), using
174 hexane/ethyl acetate 1:1, v/v as eluent. An aliquot of the IPL fraction was analyzed directly for CLs to

check for potential carry-over into the IPL fraction. In order to degrade the IPLs to CLs, half of the extract was refluxed for a minimum of 2 h in 1.5 N HCl in MeOH. The amount of CL in this IPL-derived fraction was corrected for the amount of CL brGDGTs carried-over, measured from the non-refluxed IPL fraction. All GDGTs were quantified against a known amount of C_{46} GDGT standard (Huguet et al., 2006) that was added to the CL fraction before filtration through a 0.45 μm PTFE filter and to the IPL fraction before the separation preceding the acid hydrolysis. The relative response factor of the brGDGTs was based on the relative response factor of crenarchaeol.

Samples were analyzed using a novel high performance liquid chromatography–mass spectrometry (HPLC-MS) method (De Jonge et al., 2014b). In short: GDGTs were analyzed using an Agilent 1100 series / 1100 MSD series instrument. The HPLC system was fitted with 4 Alltima Silica columns (150 x 2.1mm; 3 μm; Grace Discovery Sciences, USA) in series. Separation was achieved isocratically using 98 % hexane and 2% isopropanol (IPA) for 140 min, with a flow-rate of 0.25 $mL.min^{-1}$. After each analysis, the columns were cleaned by back-flushing hexane/IPA 1:9 (v/v), at a flow rate of 0.275 $mL.min^{-1}$, and allowed to re-equilibrate at 98 % hexane and 2% IPA for 15 min. Detection was achieved in selected ion monitoring mode (SIM; Schouten et al., 2007) using *m/z* 744 for the internal standard, *m/z* 1292 for crenarchaeol and *m/z* 1050, 1048, 1046, 1036, 1034, 1032, 1022, 1020 and 1018 for branched GDGTs. Agilent Chemstation software was used to integrate peak areas in the mass chromatograms of the protonated molecule ([M+H]+).

3.3. Calculation of GDGT-based ratios and proxies.

The isomer ratio (IR) represents the fractional abundance of the penta- and hexamethylated 6-Me brGDGTs, compared to the total of penta- and hexamethylated brGDGTs (modified after De Jonge et al., 2014a):

$$IR = (IIabc'+IIIabc')/(IIabc+IIIabc+IIabc'+IIIabc') \quad \text{[Eq. 1]}$$

The roman numerals refer to the fractional abundances of GDGTs indicated in Fig. 1, II, III are 5-Me brGDGTs, while II' and III' are 6-Me brGDGTs. Xabc means that this index includes both the non-cyclopentane containing (Xa) and the cyclopentane containing (Xb,c) components.

The BIT index was calculated according to Hopmans et al. (2004). The inclusion of 6-Me brGDGTs is mentioned explicitly:

$$\text{BIT index} = (Ia+IIa+IIIa+IIa'+IIIa')/(Ia+IIa+IIIa+IIa'+IIIa'+IV). \quad [Eq.\ 2]$$

Here, Ia is a brGDGT and IV is the isoprenoid GDGT (iGDGT) crenarchaeol (specific GDGT for Thaumarchaeota; Sinninghe Damsté et al., 2002). As the relative response factor of crenarchaeol and brGDGTs shows sigificant variation between laboratories (Schouten et al., 2013a), the absolute BIT-values might not be reproducible, but no implications for the relative changes in BIT-values are expected.

We calculated a reconstructed pH using the CBT' index following De Jonge et al., (2014b):

$$CBT' = {}^{10}\log[(Ic+IIa'+IIb'+IIc'+IIIa'+IIIb'+IIIc')/(Ia+IIa+IIIa)]. \quad [Eq.\ 3]$$

$$pH = 7.15 + 1.59 * CBT' \quad [Eq.\ 4]$$

The MAT_{mr} is calculated as a multiple linear regression (De Jonge et al., 2014b):

$$MAT_{mr}\,(°C) = 7.17 + 17.1*[Ia]+25.9*[Ib]+ 34.4*[Ic] - 28.6*[IIa] \quad [Eq.\ 5]$$

The square brackets in this formula indicate that we use the fractional abundance, i.e. the value is relative to the sum of all the brGDGTs (Ia+Ib+Ic+IIa+IIa'+IIb+IIb'+IIc+IIc'+IIIa+ IIIa'+IIIb+IIIb'+IIIc+IIIc').

3.4. Environmental parameters and bulk geochemical analysis.

The pH of the river and marine water was measured on-board. The particulate organic carbon (POC) and $\delta^{13}C$ content of river SPM on the filter was measured using a Flash 2000 Organic Elemental Analyzer. The total organic carbon (TOC) and total nitrogen (TN) content and the $\delta^{13}C$ and

$\delta^{15}N$ values from the sediments, coastal cliffs and soil samples were measured after decalcification of the sediments, in an overnight reaction with a surplus of a 1.5 N HCl solution. After washing the sediment residue with bidistilled water and re-adjusting the pH to 4-5, the freeze dried sediments were analyzed using a Flash 2000 Organic Elemental Analyzer.

3.5. Numerical analysis.

The principal component analysis based on the correlation matrix was performed using the R software package for statistical computing. We performed an unconstrained Q-mode PCA on the standardized relative brGDGT values of the core lipid fraction, for those sites that have more than 8 components quantified. The brGDGT scores are calculated proportional to the eigenvalues, and the site scores are calculated as the weighted sums of the species scores. Squared Pearson correlation coefficients (r^2 values) are reported to demonstrate the performance of the linear correlations.

4. Results

In order to constrain the sources of the brGDGTs in the Yenisei River and the Kara Sea, the brGDGT abundance and distribution is investigated. The brGDGTs encountered in the SPM and sediments of the Kara Sea can be derived from several sources; they can be soil-derived and transported by the Yenisei River, they can be produced in-situ in the river system, or delivered to the marine system through coastal erosion, or they can be of marine origin. To constrain the source of the bulk organic matter (OM; terrigenous versus marine), bulk geochemical parameters have also been measured on the SPM, sediments, coastal cliffs and soils.

4.1. Bulk parameters

Bulk geochemical parameters (OC content, N content, $\delta^{13}C_{org}$ and $\delta^{15}N$) were determined on SPM from the Yenisei River and the Kara Sea, surface sediments and coastal cliffs. The data obtained is listed in Tables 2 and 3. The sample stations are discussed according to the geographical zones (Table 1 and Fig. 2). The particulate organic carbon (POC) content (Table 2) of the Yenisei River has been reported before in De Jonge et al. (2014a), with low POC contents in the main stream (0.02-0.4

mg.L^{-1}), and higher values encountered in some upstream rivers (1.6-6.4 mg.L^{-1}). The POC content of the SPM of the Yenisei River Mouth is comparable to that of the main river (0.02-0.5 mg.L^{-1}), and remains stable throughout most of the Yenisei Gulf (0.02-0.1 mg.L^{-1}). Highest POC concentrations were encountered offshore Oliney Island (2.0-8.1 mg.L^{-1}). Marine water in the Kara Sea, sampled further offshore has a much lower POC content between 0.06 and 0.1 mg.L^{-1}.

The $\delta^{13}C_{org}$ of SPM (n=23) varies between -27.6 and -35.0‰ (Table 2). Highly variable values are encountered in the Yenisei River SPM (-27 to -35‰), and generally follow a latitudinal trend, with more negative values at higher latitudes. After the outflow in the Kara Sea no geographical trends are obvious, with $\delta^{13}C_{org}$ values varying between -28 and -33‰.

Surface sediments (n=24) were sampled from the Yenisei River Mouth on. The TOC content of the sediments varies between 0.03 to 2.5% of the dry weight, with TN values between 0.0 and 0.2% (Table 3). The highest TOC contents are encountered after the widening into the Yenisei Gulf (Fig. 2; up to 2.5%), while the Yenisei River Mouth and especially the Khalmyer Bay sediments have lower TOC and TN concentrations (0.2-1.6 and 0.0-0.1%, respectively). The Yenisei outflow sediments have an intermediate TOC concentration (1.2-1.8%), while the offshore Kara Sea sediments show a variable TOC and TN content (0.6-1.4 and 0.06-0.2%, respectively).

The sedimentary $\delta^{13}C_{org}$ values vary between -23.1 and -29.1‰ (Table 3), more positive than the $\delta^{13}C_{org}$ signal of the overlying SPM. The stable nitrogen isotopic signal varies between 2.3 and 7.9‰ (Table 3). Both the $\delta^{13}C_{org}$ and the $\delta^{15}N$ show a geographical pattern, with the lightest $\delta^{13}C$ and the heaviest $\delta^{15}N$ values encountered in the sediments from the Yenisei River Mouth and Khalmyer Bay.

The TOC and TN values of the coastal cliffs (n=10) are, in some cases, much higher compared to the marine sediments (up to 14% of the dry weight), although the majority of the measured values are comparable to the values in the marine sediments (Table 6). The TN content varies between 0.02 and 0.2%. The $\delta^{13}C_{org}$ values vary between -25.2 and -27.2‰ for the coastal cliffs along the Yenisei River Mouth, with slightly more depleted values measured in the coastal cliffs along the Yenisei River Gulf (between -26.4 and -27.2‰). The $\delta^{15}N$ values of the cliffs along the Yenisei River Mouth have a value between 1.0 and 3.6‰, while the cliffs encountered further downstream have values between 2.4 and 7.1‰. The TOC and TN content, measured on one watershed soil is significantly larger, 50% and

285 1% of the dry weight respectively (Table 6). The $\delta^{13}C_{org}$ value (-26.4 ‰) is comparable to that of the
286 coastal cliffs.
287
288 *4.2. Abundance of crenarchaeol and brGDGTs*
289 The TOC-normalized concentrations of the brGDGTs and crenarchaeol in the SPM are
290 summarized in Table 4. The concentration of crenarchaeol in the river SPM is low, varying between
291 0.02-0.3 μg.g POC^{-1}. The crenarchaeol concentrations in the Yenisei River Mouth are also low (0.2-1
292 μg.g POC^{-1}), with increased values encountered only in the Yenisei Gulf (up to 12 μg.g POC^{-1}).
293 Further downstream, marine SPM is characterized by crenarchaeol concentrations varying between 0.1
294 and 1 μg.g POC^{-1}.
295 The concentration of the summed amounts of brGDGTs in the SPM of the Yenisei River
296 exceeds that of crenarchaeol at all locations, varying between 1 and 20 μg.g POC^{-1} (Table 4). This is
297 reflected in high BIT-values, varying between 0.93 and 0.99 (Table 4). The brGDGT concentrations in
298 the Yenisei River Mouth SPM (i.e. 20-40 μg.g POC^{-1}) are high compared to the concentrations
299 observed in the Yenisei River SPM. In the Yenisei Gulf the concentrations are lower on average, but
300 highly variable (5-40 μg.g POC^{-1}). Further downstream, the concentrations decrease to only 0.1 μg.g
301 POC^{-1}. The BIT values decrease from over 0.95 in the Yenisei outflow down to 0.22 in marine SPM
302 (Fig. 3A; Table 4).
303 The TOC-normalized concentration of crenarchaeol in the sediments (Table 5) shows a clear
304 geographical distribution, with the lowest values (0.2 to 1.3 μg.g TOC^{-1}) encountered in the Yenisei
305 River Mouth, while sediments of the Kara Sea have crenarchaeol concentrations of up to 33 μg.g TOC^{-1}.
306 The brGDGT concentration in the sediments is highest in the Yenisei River Mouth (36 to 87 μg.g
307 TOC^{-1}), decreasing to an average of 11 μg.g TOC^{-1} in Kara Sea sediments (Table 5). The BIT values
308 decrease from 0.98 in the Yenisei River Mouth to 0.76 in the Yenisei Gulf and decrease further to 0.09
309 in the open marine sediments (Fig. 3B; Table 5).
310 Although the Khalmyer Bay is not part of the flow path downstream the Yenisei River, GDGT
311 concentrations are comparable to the Yenisei River Mouth both for SPM and surface sediments.
312 BrGDGT concentrations in SPM vary between 20 and 50 μg.g TOC^{-1} with substantially lower

crenarchaeol concentrations, resulting in BIT values of over 0.95 (Table 4). The crenarachaeol concentration is low in the Khalmyer Bay sediments (0.7 to 1.0 μg.g OC^{-1}), increasing further downstream in the Khalmyer Gulf (11 to 12 μg.g TOC^{-1}) (Table 5). The brGDGT concentration is high in the Khalmyer Bay sediments (50 to 80 μg.g TOC^{-1}), again resulting in high BIT values (0.98-0.99) (Table 5).

The brGDGT concentration in the coastal cliffs (Table 6) varies between 8 and 50 μg.g TOC^{-1}, with crenarachaeol abundances varying between 0.02 and 10 μg.gTOC^{-1}. The resulting BIT-values vary between 0.71 and 1.00 (Table 6). The BIT-values in the watershed soils are also high (1.00), with the highest amount of brGDGTs in this dataset encountered at the site S_2 (86 μg.gTOC^{-1}).

4.3. Distribution of brGDGTs

The fractional abundances of brGDGTs are reported in Tables 4, 5, and 6, for SPM, sediments and coastal cliffs and watershed soils, respectively. Fig. 4 shows the brGDGT distribution encountered in the Yenisei river and downstream samples, averaged per sampling zone, of those samples that have >8 compounds quantified. Fig. 5A-C shows the brGDGT distribution averaged for the Khalmyer Bay and Gulf SPM and sediments. Furthermore, Fig. 5D-F shows the brGDGT distribution in the Kara Sea coastal cliffs and in the 2 watershed soils analysed. The brGDGTs present in the CL and IPL fractions are quantified separately. As the IPL brGDGTs are rapidly degraded in the environment (White et al., 1979), they can be interpreted to be indicative of living or recently living material, although archaeal IPL GDGTs with glycosidic head groups have been found fossilized in deeply buried sediments as well (Lengger et al., 2014).

The average brGDGT distribution of the Yenisei River SPM shows a dominance of the 6-Me brGDGTs (Fig. 4A; >50% of summed brGDGTs) as reported previously for the 6-Me hexamethylated brGDGTs (De Jonge et al., 2014a). The IPL fraction, comprising on average 6% of the total brGDGT pool, has a similar average distribution as the CL fraction (Fig. 4E). In contrast, in the most offshore site, the Kara Sea, both the SPM and the CL and IPL fractions of the surface sediments are dominated by the 5-Me brGDGTs (Fig. 4D, K, O; >75% of brGDGTs). Furthermore, these sites show a strong increase of the fractional abundance of brGDGT Ia. While the amount of IPLs in the SPM at these

341 sites is below detection limit, the relative abundance of IPLs in the Kara Sea sediments is 9% of total
342 brGDGTs on average. The distribution encountered in this fraction is similar to the CL brGDGTs
343 (Figs. 4K and 4O). The CL fraction of both the SPM and sediments of the Yenisei River Mouth,
344 Yenisei Gulf and Yenisei Outflow, show a brGDGT distribution that is an intermediary of the Yenisei
345 River and Kara Sea distributions. Moving downstream, we observe decreasing fractional abundances
346 of 6-Me brGDGTs, and increasing fractional abundances of brGDGT Ia (Fig. 4B, C, H, I, J). At these
347 sites, the relative abundance of IPL brGDGTs in the SPM varies between 0 and 5%, with the majority
348 of the sites having IPL brGDGTs present below detection limit. While the IPL distribution in the
349 Yenisei River Mouth mimics the CL distribution (Fig. 4F), the distribution of IPL brGDGTs in the
350 Yenisei Gulf (Fig. 4G) is quite different from that of the CL brGDGTs (Fig. 4C), with increased
351 amounts of the hexamethylated brGDGTs. The amount of IPLs in the sediments is higher, on average
352 6%, although no major differences between the sedimentary CL and IPL brGDGT distributions are
353 observed.

354 In the sedimentary brGDGT distribution in Khalmyer Bay and Gulf (Fig. 5A, C), both the CL
355 and IPL fractions are dominated by 5-Me penta- and hexamethylated brGDGTs (Fig. 5C). IPL
356 brGDGTs could only be quantified in the sediments, varying between 5 and 11% of total brGDGTs.
357 The distribution in the coastal cliff samples that border the Yenisei River Mouth and Gulf is
358 summarized in Fig. 5D. Again, the 5-Me penta- and hexamethylated brGDGTs IIa and IIIa are the
359 most abundant compounds and, in general, the distribution is rather similar to those of the Khalmyer
360 Bay and Gulf (Fig. 5).

361 Only two watershed soils were available for analysis, and neither of these soils represents a
362 'typical' topsoil (0-10 cm; De Jonge et al., 2014b). The first sample was collected in a lake's
363 floodplain, and is characterized by a dominance of brGDGT IIIa, IIIa' and IIa (Fig. 5E). The second
364 sample was collected in an outcrop, 1.95m below the surface of a peat layer. This sample is
365 characterized by a very large abundance (65%) of the tetramethylated brGDGT Ia (Fig. 5F).

366 To investigate the changes in distribution of the 15 brGDGTs per site, we performed a principal
367 component analysis (PCA) on the standardized fractional abundances of the CL brGDGTs at all
368 studied sites, including the Khalmyer Bay, coastal cliff samples and watershed soils (Fig. 6A, C). We

excluded samples that have <9 brGDGTs quantified (n=8), mostly due to samples with low brGDGT abundances, to avoid a bias in the PCA. The first three principal components (PC) explain a large part (37, 29 and 13%, respectively) of the variance. The scores provide a summary of the relationship between the stations and the variables (Fig. 6B, D). The strong inverse correlation between the 6-Me brGDGTs IIa', IIb', IIIa', IIIb' and IIIc' on the one hand, and the 5-Me brGDGTs IIa and IIIa on the other hand is captured well by the first principal component (Fig. 6A). This inverse correlation is confirmed by the correlation coefficients (r^2) between the fractional abundances of IIa and IIa' (r^2=0.70, $p<0.05$), and, to a lesser extent, between IIIa and IIIa' (r^2=0.23, $p<0.05$). Scores on the second PC are predominantly determined by the fractional abundance of a number of minor, cyclopentane containing brGDGTs (i.e. Ib, Ic, IIb, IIc, IIIb, IIIc and IIc'). The third PC (Fig. 6B) is determined by the fractional abundance of brGDGT Ia, that follows an inverse trend as the fractional abundance of brGDGTs IIc, IIIa, IIIb and IIIc, on PC3. We can evaluate downstream trends in the distribution of the 15 brGDGTs by evaluating the scores of the sample sites on these three principal components.

The low scores on PC1 of the Yenisei River SPM (-0.9; Fig. 6B) is in line with the increased abundance of brGDGTs IIa' and IIIa', and consistent with their high IR (0.46-0.77). Compared with the Yenisei River, a strong shift in the brGDGT distribution can be observed in samples collected in the marine system. They show an increasingly higher score on PC1 (except for the Yenisei Outflow and one Kara Sea sediment), indicating a strong shift in the abundance of the 6-Me brGDGTs IIa' and IIIa' (Fig. 6B, E). This is accompanied by lower scores on PC2, related to the increase of the relatively less abundant cyclic brGDGT compounds (i.e. Ib, Ic, IIb, IIc, IIIb, IIIc and IIc'). This decrease of the scores on PC2 is gradual; the SPM and sediments from the Yenisei river Mouth and Gulf score weakly positive, whilst the score on PC2 is negative for the Kara Sea sediments (Fig. 6F), including those sites that underlie the Yenisei River (and Ob River) plume. The scores on PC3 (Fig. 6D, G), mainly reflecting the fractional abundance of brGDGT Ia, increase in the offshore marine Kara Sea sediments (Sed=1.2 and SPM=1.4). This is also the case for the Yenisei Outflow sediments (0.8) and to a lesser degree for the Yenisei Gulf sediments and SPM.

396 The scores on PC1 (Fig. 6B) of both the Khalmyer Bay and Gulf SPM and sediments indicate
397 an increased amount of the fractional abundance of the brGDGTs IIa and IIIa (Sed = 0.6, SPM = 0.5;
398 Fig. 6B). Compared to the Khalmyer Bay, the Khalmyer Gulf samples also have a relatively higher
399 score on PC2 (Sed = -0.2 and SPM = -0.3), reflecting an increased abundance of cyclopentane-
400 containing brGDGTs. Both the Khalmyer Bay and Gulf samples have a low score on PC3 (Sed = -0.8
401 and SPM = -0.3), indicating that the fractional abundance of brGDGT Ia is not increased in these
402 samples (Fig. 6D).
403 The samples collected from the Kara Sea coastal cliffs show a rather variable brGDGT
404 distribution. However, the high scores on PC1 indicate that the high fractional abundances of the 6-Me
405 brGDGTs IIa' and IIIa' encountered in the river SPM, are not encountered in the coastal cliffs (Fig.
406 6D). The distributions spans the majority of the variance on PC2, while their low values on PC3 (0.0
407 on average) indicate that the increased fractional abundance of brGDGT Ia is not encountered in the
408 coastal cliff samples. Both watershed soils have a very different distribution, with the mountainous
409 peat scoring slightly negatively on PC1, contrasting with the positive score of the lowland peat. Both
410 sites have similar scores on PC2, but especially the score on PC3 is radically different, while the
411 mountainous peat has a negative value, the lowland peat has the highest score on PC3 of this dataset.
412
413 **5. Discussion**
414 *5.1. Sources of riverine brGDGTs*
415 In order to use sedimentary brGDGT lipids in palaeoclimate reconstructions, it is essential that
416 the distribution of the brGDGTs does not change between the formation of the signal in soils, their
417 transport through a river system following soil erosion, and their sedimentation in the marine or
418 lacustrine system. In our previous study of the brGDGTs in the Yenisei River SPM (De Jonge et al.,
419 2014a) it was concluded that the majority of the brGDGTs in the Yenisei River SPM were in-situ
420 produced, based on the fact that the reconstructed MAT and pH fitted poorly with the soil pH and the
421 MAT imposed on the watershed. However, we employed a soil calibration by Peterse et al. (2012) that
422 was based on a dataset where the 5- and 6-Me brGDGTs were not individually quantified, while the
423 hexamethylated 6-Me brGDGTs were shown to be abundant in the Yenisei River SPM. Re-analysis of

424 the Yenisei SPM samples now allows separating six 6-Me isomers and quantifying all 15 brGDGT
425 components (De Jonge et al., 2014b). The fractional abundance of 6-Me brGDGT in soils increases
426 strongly with increasing pH (De Jonge et al., 2014b). As they are present in high abundance (>50% of
427 summed brGDGTs; Fig. 4) in the Yenisei River water SPM, the novel pH calibration (Eq. 3 and 4; De
428 Jonge et al., 2014b) results in pH values between 6.9 and 7.9 pH units. This is similar to what was
429 obtained previously with the Peterse et al. (2012) calibration, and is significantly higher than the soils
430 present in the Yenisei watershed (De Jonge et al., 2014a). The river water pH values (7.2-7.3) are
431 reconstructed well, taking the calibration's residual standard mean error (RSME) of 0.5 into account.
432 This confirms the dominant influence of aquatic in-situ production on the brGDGT distributions in the
433 Yenisei River. The reconstructed MAT, based on the novel MAT_{mr} (Eq. 5; De Jonge et al., 2014b)
434 varies between 3.5 and 7.1 °C. This is on average 4 °C warmer than the reconstructed MAT using the
435 Peterse et al. (2012) soil calibration and on average 9 °C warmer than the measured MAT in the
436 Yenisei watershed. As the calibration by De Jonge et al. (2014b) significantly overestimates the MAT
437 of cold soils, the temperature offset alone is not sufficient to identify the brGDGTs as riverine in-situ
438 produced. However, a large temperature gradient is imposed on the watershed soils (De Jonge et al.,
439 2014b), that is absent in the reconstructed temperatures, and it is primarily the lack of this gradient,
440 together with the deviating reconstructed pH values, that indicate that the watershed soils are not the
441 dominant source of riverine brGDGTs in the late summer. Therefore, the conclusion from De Jonge et
442 al. (2014a) that the Yenisei River brGDGTs are dominantly produced in-situ remains valid.
443
444 *5.2. Sources of brGDGTs in the Yenisei River Mouth and Gulf*
445 The variation in the brGDGT distribution of the SPM and sediments was analysed using a
446 principal component analysis (PCA; Fig. 6). The Yenisei River SPM, especially in the lowland river,
447 has a large fractional abundance of 6-Me brGDGT IIIa' and IIa' (Fig. 4). The high abundance of these
448 brGDGTs, whose fractional abundance was shown to increase with increasing soil pH (De Jonge et al.,
449 2014b), reflects their production in the neutral pH of the Yenisei River water. However, the brGDGTs
450 distribution delivered by the Yenisei River is altered significantly in the Yenisei River Mouth and in
451 the Kara Sea. Firstly, considering the scores on PC1 (Figs. 6B, 6E), both SPM and sediments in the

Yenisei River Mouth show a strong decrease in the fractional abundance of the brGDGTs IIIa' and IIa', compared to the upstream Yenisei River values. Also the scores on PC2 (Figs. 6B, 6F) indicate a shift in the brGDGT distribution between the Yenisei River SPM and Yenisei River Mouth. Furthermore, shifts in the brGDGT distribution are observed further downstream the Yenisei River Mouth, in the Yenisei Outflow, but also in the Kara Sea samples that are not directly influenced by the Yenisei Outflow (KS1-KS4). The scores on PC2 decrease for the Yenisei Outflow and some of the Kara Sea samples. Considering the scores on PC3 (Figs. 6D, 6G) we see that the fractional abundance of brGDGT Ia increases downstream from the Yenisei River Mouth samples. This increase happens gradually, first in the Yenisei Gulf, and further in the Kara Sea sediments and SPM (Fig. 6G).

5.2.1. BrGDGTs delivered by the Yenisei River

Although the brGDGT distribution in the lowland Yenisei River is stable throughout August/September, the contrasting brGDGT signature in the Yenisei River Mouth, compared to the signature in the upstream Yenisei River SPM, possibly reflects brGDGTs that were delivered to the marine system earlier in the year. The SPM of the Yenisei River analysed in this study only represents a snapshot in time and may be quite different from the brGDGT composition of SPM transported by the flood that results from snowmelt during the months May-June. Indeed, the majority of terrigenous OM is thought to be supplied to the Kara Sea during the freshet (Lisitsyn, 1995) and the freshet SPM is possibly much more enriched in brGDGTs, as was recently reported by Peterse et al. (2014b) for the Kolyma River (Eastern Siberia), where a 10 times increased amount of brGDGTs was measured during the freshet, compared to the base flow (50 days later), and even a 30-fold increase compared to the season with ice-cover. Large temporal differences in the SPM brGDGT concentration were also observed in the Arctic MacKenzie river, although the highest TOC-normalized values were not only observed during the freshet (Peterse et al., 2014b). As the freshet is accompanied by large amounts of horizontal run-off and soil erosion, the SPM delivered during this period may carry brGDGTs that are more influenced by a contribution of soil-derived brGDGTs. Although this material was delivered to the Yenisei River Mouth several months prior to our sampling campaign, it may still be present as a background signal in the Yenisei River Mouth SPM. Indeed, Gaye et al. (2007) concluded that the

main settling fluxes to the sediments do not occur during the freshet, but rather during the months with decreased flow speed (September/October), and especially during the months with ice cover. This is because OM delivered during the freshet will remain in suspension until the flow speed has decreased sufficiently to allow settling of the particles. The material delivered during the freshet is thus still in suspension, or may have been resuspended (Gaye et al., 2007). The presence of brGDGTs that were delivered to the Yenisei River Mouth since the start of the freshet results in a suspended brGDGTs distribution that is an average of the OM delivered since May. This probably explains why the brGDGT distribution in the surface sediments, that is an average of the settling particle flux over several years, has similar brGDGT distribution as the overlying SPM (Fig. 6C, E). Also the comparable OC-normalized abundances of the brGDGTs indicate a strong coupling between the SPM and sediments in this shallow setting.

Unfortunately, as the brGDGT distribution in the Yenisei River during the freshet is unknown, constraining the amount of riverine and soil-derived brGDGTs in the Yenisei River Mouth is not possible. Although the fractional abundance of 6-Me brGDGTs IIa' and IIIa' decreases compared to the Yenisei River SPM, increased abundances are still encountered in the Yenisei Mouth SPM and sediment, suggesting that at least part of the brGDGT signal is derived from riverine in-situ production.

5.2.2. BrGDGTs derived from coastal cliffs

In contrast to many other coastal seas around the globe, the shoreline of the Kara Sea is composed of an extensive system of coastal cliffs that are subjected to thermal and wave erosion. These thermoabrasive coasts are frozen for most of the year, with intensive erosion occurring only during the summer months. The Kara Sea coastal cliffs (up to 80 m high) are comprised mainly of Pleistocene marine sandy clays, with only little contribution of continental soils (Streletskaya et al., 2009). In the Kolyma River Basin, a Northeastern Siberian shelf sea similar to the Kara Sea, coastal OM was shown to contribute to 50-60% of surface sediment OM (Vonk et al., 2010). However, Streletskaya et al. (2009) estimate that the amount of OM delivered by coastal erosion into the Kara Sea (defined as the area between Nova Zemblya and Taymyr Peninsula), is about 25 times less than

508 the amount delivered by the rivers. The Khalmyer Bay and Gulf exemplify a setting in the Kara Sea
509 area where the majority of brGDGTs encountered could be primarily derived from coastal cliff
510 erosion, as no major rivers drain into this bay. Although no erosion rates of the coastal cliffs are known
511 for this setting (Lantuit et al., 2012), satellite photos (e.g. Fig. 2A) show that the amount of clastic
512 material deposited in this bay is substantial. Indeed, high concentrations of brGDGTs, coeval with high
513 BIT-values, were encountered in the Khalmyer Bay (Fig. 3D). Although quite variable in composition,
514 the weighted average of the brGDGT distribution of the Kara Sea coastal cliffs (red asterisk in Figs.
515 6B-D) is similar to the brGDGT distributions encountered in Khalmyer Bay SPM and sediments (cf.
516 Fig. 5D and Figs. 5A-B). Assuming a similar brGDGT distribution for the cliffs of Khalmer Bay as for
517 the cliffs in the Yenisei River Mouth and Gulf, this strongly suggests that coastal cliffs may be a major
518 source for brGDGTs in the Khalmyer Bay area.
519 The brGDGTs encountered in the Yenisei Mouth and Gulf, on the other hand, will reflect a
520 mixture of riverine and coastal sources. Slow erosion rates (i.e. 0.2 to 0.4 $m.yr^{-1}$) are reconstructed for
521 the coastal cliffs at the latitude of YM1, where the coastal cliffs have a height between 20 and 40 m
522 (Streletskaya et al., 2009), while the northeastern coastline of the narrow in the Yenisei Mouth (i.e.
523 Sopochnaya Karga ice complex; in the proximity of sample sites YM2-YM5), was shown to be a site
524 with moderate erosion rates, in the order of 1-2 m yr^{-1} (Lantuit et al., 2012). BrGDGTs derived from
525 coastal cliffs may thus have an influence on the brGDGT distribution, although the extent to which
526 this influences the brGDGT distribution encountered in the Yenisei River Mouth and Gulf is unknown.
527
528 *5.3. Sources for brGDGTs in the Yenisei Outflow in the Kara Sea*
529 The brGDGT distribution encountered in the Yenisei River Mouth is a mixture of riverine in-
530 situ produced brGDGTs, an unknown contribution of soil-derived brGDGTs delivered by the river
531 during the freshet, and an unknown contribution of coastal-cliff derived brGDGTs delivered to the
532 marine system following coastal erosion. This complex mixture is transported eastwards, under the
533 influence of the Greenland current (Fig. 2C). Another major source of brGDGTs in the Kara Sea
534 system is the Ob River. The brGDGT distribution delivered by the Ob River, sampled downstream the
535 Ob Gulf, is similar to some of the Yenisei Gulf distributions (Figs. 6B, 6D), reflecting similar brGDGT

sources, as can be expected by the similar geographical extent of the Ob River. We note that the Kara Sea locations (KS1-4) that are not directly under the influence of the Yenisei River plume probably indirectly receive brGDGTs from the Yenisei River and Ob River outflow, through the anti-clockwise surface current present in the Kara Sea (Fig. 2).

Although the complex origin of the brGDGT mixture in the Yenisei Mouth and Gulf cannot be resolved, this is not the final distribution encountered in the Yenisei Outflow SPM and surface sediments. Moving downstream, we observe a simultaneous decrease of the brGDGT concentration and a shift in the brGDGT distribution, that is reflected in the changing values along PC2 and PC3 (Figs. 6F-G). The largest change is the increase in the fractional abundance of brGDGT Ia in the sediments (up to 43% of all brGDGTs; correlation with distance river Mouth: $r^2 = 0.75$). Also, the concentration of summed brGDGTs decreases strongly downstream of the Yenisei River (negative correlation with distance river Mouth: $r^2 = 0.42$). A mechanistic link between the changing brGDGT distribution and the amount of brGDGTs, or the distance from the river Mouth, seems apparent.

We discuss two mechanisms that may be responsible for changing brGDGT distributions in an increasingly marine system. The first is in-situ production of marine brGDGTs. This mechanism has been invoked by a number of authors to explain changing brGDGT distributions in marine coastal sediments (Svalbard fjord, Peterse et al., 2009; Yangtze River, Zhu et al., 2011; Pearl River, Zhang et al., 2012; Tagus River and Amazon River; Zell et al., 2014a,b). Overall, these authors describe an increase in the fractional abundance of one or more cyclopentane-containing brGDGTs. The effect of in-situ production on the Kara Sea system is probably captured along the second PC, reflected in the increase of a group of minor, cyclopentane-containing brGDGTs, that affect the brGDGT distribution of the Yenisei Outflow and Kara Sea samples (Fig. 6B). The values on PC2 decrease with increasing distance to the Yenisei River, where the Kara Sea samples that are less influenced by the Yenisei Outflow signal are characterized by the lowest values. Especially the deepest site, KS4, seems to be influenced by an increase of both minor 5-Me cyclopentane-containing brGDGTs (low values on PC2; Fig. 6F), which generally increase with increasing pH, and 6-Me brGDGTs (low values on PC1; Fig. 6E), that have been shown to increase with increasing soil pH (De Jonge et al., 2014b). More information concerning the in-situ produced signal can be derived from the intact polar lipid (IPL)

fraction. The brGDGTs from living or recently living cells will be present as IPLs, which, after cell death are rapidly degraded into core lipids (CL). The relative abundance of the IPL brGDGTs in the Kara Sea sediments is high (average: 9%), comparable to the IPL percentage in soils (eg. 9-19%; Peterse et al., 2010) and the fractional abundance of the cyclopentane-containing brGDGTs in the sedimentary IPL fraction is slightly larger than in the CL fraction (25% versus 18% for Yenisei outflow samples, 18% versus 14% for Kara Sea samples).

However, the encountered brGDGT distribution in the Yenisei Outflow and Kara Sea SPM and sediments, cannot be fully attributed to in-situ production. In-situ produced marine brGDGTs in high-latitude marine sediments were observed by Peterse et al. (2009) in sediments offshore Svalbard. As Svalbard is located at the same latitude as the most offshore samples in the Kara Sea, we expect an in-situ produced marine brGDGT distribution to be comparable, assuming that other environmental factors, such as the trophic status of the sediments, only play a minor role. However, the brGDGT distribution Peterse et al. (2009) observed in Svalbard fjords is clearly distinct from the distributions in the Yenisei outflow system. The Svalbard in-situ produced distribution reflects the relatively high pH of the Arctic Ocean, resulting in a brGDGT distribution that was dominated by cyclopentane-containing brGDGTs (60 % of total brGDGTs), in contrast to the off-shore Kara Sea sediments, where the cyclopentane–containing brGDGT comprise on average 14% and at maximum 23% of total brGDGTs. Furthermore, the in-situ produced signal in the Arctic sediments off Svalbard reflects the cold conditions with hexa- and pentamethylated brGDGTs representing 88% of the total, while these highly methylated brGDGTs in the offshore Kara Sea sediments amount up to between 55 and 63%. Thus, although in-situ production influences the Kara Sea sedimentary brGDGT distribution (as reflected by PC2), it does not fully explain the encountered brGDGT distribution. Especially the increase in the fractional abundance of a ‘warm’ tetramethylated brGDGT, representing up to 42% of all brGDGTs (as also reflected by the high scores on PC3; Fig. 6G) cannot be attributed to in-situ produced marine brGDGTs. Furthermore, the fractional abundance of brGDGT Ia is not increased in the IPL fraction compared to the CL fraction (29% versus 32% for the Yenisei Outflow, 36% versus 38% for the Kara Sea samples), indicating that this brGDGT is probably not in-situ produced.

591 The strong correlation between the fractional abundance of the tetramethylated brGDGT Ia (r^2 =
592 0.75) and the distance from the river mouth suggests preferential degradation as a possible explanation
593 for the observed shifts in brGDGT distribution. Preferential degradation could affect brGDGT
594 distributions in two different ways. Firstly, degradation may change the brGDGT distribution if
595 individual brGDGTs (i.e. with a different number of methyl substituents) would possess a different
596 reactivity. This is, however, not likely, as a study on the degradation of OM in a oxidized turbidite
597 (Huguet et al., 2008) did not indicate changes in the distribution of the brGDGTs that are comparable
598 to those observed in the Kara Sea transect. Secondly, degradation can cause changing brGDGT
599 distributions through preferential degradation of different brGDGT pools. The brGDGTs present in the
600 Yenisei River Mouth are a mixture of an in-situ produced riverine signal and an unknown amount of
601 less labile brGDGTs, both derived from the river watershed and the coastal cliffs. When a mixture of
602 pre-aged and modern (river-derived) OM is delivered to the marine system, the riverine fraction is
603 more labile and will be degraded preferentially (e.g. Blair and Aller, 2012). This is because less labile
604 soil-derived material and fossil material, associated with clay particles, will be physically protected
605 from degradation (Hedges and Keil, 1995; Keil and Mayer, 2014, and references therein). Thus, the
606 contribution of riverine in-situ produced brGDGTs to the Yenisei Outflow and Kara Sea distributions
607 is assumed to be minor. This is also indicated by the offset between the brGDGT distributions
608 encountered in the Yenisei River SPM and the Yenisei Outflow (Fig. 6B, 6D).
609 Both the watershed soils and coastal cliffs can be the source of the brGDGTs encountered in the
610 Yenisei Outflow and Kara Sea. We postulate that a coastal cliff source is less probable, as a large offset
611 is observed between the brGDGT distribution present in the coastal cliffs and in the Yenisei Outflow
612 (Fig. 6B, 6D). Secondly, making a rough estimate of the relative contribution of coastal cliff brGDGTs
613 to the total Kara Sea brGDGT pool reveals that coastal-cliff derived brGDGTs represent only a small
614 fraction of the total brGDGTs delivered to the Kara Sea system. Based on the OC content measured in
615 the cliffs and the erosion rate, estimates of the amount of OM delivered into the Kara Sea (defined as
616 the area between Nova Zemblya and Taymyr Peninsula) have been made by Streletskaya et al. (2009).
617 These estimates indicated that the amount of OM delivered by coastal erosion to the Kara Sea is about
618 25 times less than the amount of OM delivered by the rivers. Comparing the brGDGT TOC-

normalized concentration in the coastal cliffs with the concentration measured in the Yenisei River allows estimating the relative contributions of both sources to the total Kara Sea brGDGTs. The TOC-normalized concentration of the Yenisei Mouth coastal cliffs (n=10, on average 28 μg.gTOC^{-1}, between 8 and 51 μg.gTOC^{-1}) slightly exceed the concentration of the Yenisei River baseflow SPM (on average 12 μg.gTOC^{-1}, up to 20 μg.gTOC^{-1}). However, this is only a poor estimate of the riverine brGDGT input, as the river SPM does not carry a constant signal year-round and the POC-normalized amount of brGDGTs has been observed to increase during the freshet in another Siberian river system (e.g. Peterse et al., 2014b). Furthermore, we have no information on the concentration of brGDGTs within the Ob River SPM, and thus have to assume a similar contribution as the Yenisei River. As the amount of OC derived from rivers exceeds the coastal cliff-derived OC 25-fold (Streletskaya et al., 2009), we can thus make a conservative estimate that the contribution of brGDGTs delivered to the Kara Sea system by river will be at least 10 times more than the coastal cliffs input, based on a Yenisei River SPM snapshot that does not reflect freshet conditions.

We thus postulate that the brGDGT distribution in the Kara Sea is probably dominated by soil-derived brGDGTs. However, only two watershed soils have been analysed up to date, a mountainous peat sampled in the floodplain of a lake and a lowland peat that was sampled in an outcrop above a buried glacier (Karpov, 1983; Shpolyanskaya, 2003). Although this dataset definitely does not represent a good coverage of the Yenisei watershed soils, it does highlight that watershed soils are a potential source for the brGDGT distribution encountered offshore. Fig. 5 shows the fractional abundance of the brGDGTs encountered in these samples. While the mountainous peat (Fig. 5E) has a brGDGT distribution that is rather different from the offshore distribution (Fig. 4 D, J, K, N and O), the lowland peat sample is characterized by a large fractional abundance of Ia (65%; Fig. 5F), resulting in a fairly comparable distribution as the offshore samples. Although the extent of this potentially less labile soil type is unknown, its contribution to the Yenisei River SPM may explain the observed shift in offshore brGDGTs. In case the brGDGTs encountered in the offshore Kara Sea samples are soil-derived, we would expect that the bulk OM proxies indicate the presence of a terrigenous signal. The following section will discuss how the BIT-index performs as a tracer for

terrigenous input, and whether the presence of a terrigenous fingerprint in the sediments and SPM of the Yenisei Outflow and Kara Sea is confirmed by the bulk OM parameters.

5.4. Comparing proxies for terrigenous input in the Kara Sea

The Yenisei River delivers large amounts of OM to the Kara Sea, between 4-5 . 10^{12} g . yr^{-1} (Telang et al., 1990; Lobbes et al., 2000). The supply of OM to the marine system can possibly be traced spatially and reconstructed through time using the GDGT-based BIT-index (Hopmans et al., 2004). This ratio [Eq. 2] calculates the amount of five major brGDGT lipids relative to the amount of crenarchaeol, a membrane lipid that is specific to Thaumarchaeota and is predominantly produced in the marine system (Sinninghe Damsté et al., 2002). As the brGDGTs within the Yenisei River, several months after the freshet, were shown to be dominantly in-situ produced (De Jonge et al., 2014a), the BIT index in the Yenisei River outflow should be interpreted as a proxy for both terrigenous and riverine OM transported by the river, rather than soil-derived OM alone. Furthermore, coastal cliff-derived brGDGTs can also be significant, especially in those settings without major river input.

Although the brGDGT distribution in the Yenisei River SPM reflects an aquatic source, the BIT values of the SPM are close to unity (0.93-0.99; Table 4) and are thus comparable with values typically encountered in soils (generally >0.9; Schouten et al., 2013b). Although the contribution of brGDGT derived from the river SPM, watershed soils and coastal cliffs cannot be constrained well in the Yenisei River Mouth, all these sources have high BIT-values, resulting in Yenisei River Mouth SPM samples having similar, high BIT values (0.97-0.98).

To evaluate whether the BIT-index is governed by changes in the abundance of crenarchaeol, or by the summed abundance of brGDGTs, previous authors (e.g. Sinninghe Damsté et al., 2012; Smith et al., 2012) have evaluated whether significant correlations can be found with the concentration of these compounds. However, obtaining a significant correlation between the BIT index and the amounts of crenarchaeol and brGDGTs of the SPM is complicated by the phenomenon that some sites with intermediate BIT-values (offshore Oliney Island and in the Yenisei Gulf) have distinctly increased crenarchaeol and brGDGTs concentrations (Fig. 3C). Thus, the correlations of BIT with the abundance

673 of crenarchaeol and the summed abundances of brGDGTs have low r^2 values of 0.13 and 0.16,
674 respectively.

675 In the sediments, the BIT values mimic the pattern observed in the overlying SPM well,
676 decreasing from 0.98 in the Yenisei River Mouth to 0.09 in the offshore marine sediments (Fig. 3B;
677 Table 5). Besides the Yenisei River Mouth, also Khalmyer Bay is characterized by high BIT values
678 (0.95-0.97; Fig. 3B), reflecting the high BIT values in the Khalmyer Bay SPM. Supporting its
679 application as a tracer for terrigenous brGDGTs, the sedimentary BIT values correlate with brGDGT
680 concentration in the sediments (r^2= 0.52; Fig. 3D). However, the BIT-index also correlates negatively
681 with the crenarchaeol concentration (r^2= 0.72; Fig. 3D), indicating that both changes in crenarchaeol
682 and brGDGTs concentration influence the calculated BIT-values. This result is similar to a study
683 tracing terrigenous OM offshore Portugal by Zell et al. (2014a).

684 To further support the use of the BIT-index for reconstructing terrigenous input in the Yenisei
685 sediments, we compare the BIT values with bulk parameters that have been used to trace the input of
686 terrigenous OM in Kara Sea sediments: stable isotopes ($\delta^{13}C_{org}$) and C/N ratios (Fernandes and Sicre,
687 2000; Krishnamurty et al., 2001; Galimov et al., 2006). These studies invoked two sources for OM
688 encountered in the Kara Sea sediments, with contrasting $\delta^{13}C_{org}$ and C/N values; soil-derived
689 terrigenous matter (-27‰ and >15, respectively) and in-situ produced marine OM (-16 to -19‰ and
690 <6.5, respectively). The influence of coastal cliffs ($\delta^{13}C_{org}$ (-26.6 to -24.4 ‰) and C/N signature
691 (median=12)) was previously not taken into account. However, as the $\delta^{13}C_{org}$ values confirm a mixed
692 terrigenous and marine OM source, they can't be identified as a third end-member based on their bulk
693 OM characteristics unless radiocarbon ages are taken into account (cf. Vonk et al., 2010).

694 The stable isotopic signal of the terrigenous end-member was based on the stable isotopic signal
695 of tundra soils (Naidu et al., 1993; -27‰), and on the $\delta^{13}C_{org}$ value of the lowland peat in this study (-
696 26.4‰). Compared to these values, the $\delta^{13}C$ values of the downstream riverine SPM are distinctly
697 more negative. This is probably because of a contribution of riverine phytoplankton with strongly
698 negative values (-32 to -23‰; Michener and Lajtha, 2007). The $\delta^{13}C_{org}$ values of the sediments in the
699 Yenisei River Mouth (-26 to -29‰) agree with that of the terrigenous end-member. The sediments
700 further downstream reveal an increasing $\delta^{13}C_{org}$ value, up to -23‰ (Fig. 3D). This latter value is still

701 distinct from the marine Kara Sea end-member calculated in previous studies (Fernandes and Sicre,
702 2000; between -16 and -19‰), suggesting that even the most offshore sediments do not represent a
703 setting with an exclusively marine input of OM.

704 The C/N ratios of the sediments vary between 6.5 and 15, in agreement with previous studies
705 (Fernandes and Sicre, 2000; Krishnamurthy et al., 2001). The C/N ratio in the Yenisei River Mouth
706 sediment varies between 15.0 and 11.6, which agrees with the value of 13.5 Krishnamurthy et al.
707 (2001) obtained at this site, although the range we observe between the values is substantial.
708 Especially station YM4 seems to be characterized a strong terrigenous signal, with a $\delta^{13}C_{org}$ value of -
709 29‰ and a C/N ratio of 15. Yenisei Gulf values vary between 6.5 and 12.1, with lower values (6.5-9.3)
710 encountered offshore Oliney Island. The Kara Sea sediments west and north of the Ob and Yenisei
711 outflow (KS2, KS3, KS4), have slightly lower C/N values (7.5 to 8.1) that indicate an increased
712 amount of marine OM, although the C/N ratio confirms that even these sediments do not reflect an
713 exclusive marine OM input (C/N ratio <6.5). The Kara Sea sediments under influence of the Ob and
714 Yenisei outflow (YO and OO) have a relatively high C/N ratio (8.5-11.2) that indicates a more
715 substantial input of terrigenous OM, compared to the results from more offshore locations obtained by
716 Krishnamurthy et al. (2001) and Fernandes and Sicre (2000). Thus, both the $\delta^{13}C_{org}$ and C/N values
717 indicate the presence of terrigenous matter in offshore Kara Sea sediments, even in those sediments
718 that are not directly influenced by the Ob and Yenisei plume (i.e. KS1 - KS4). In the Khalmyer Bay
719 sediments, bulk terrigenous proxies indicate a substantial amount of terrigenous OM. Its sediments are
720 characterized by $\delta^{13}C_{org}$ values of -27.0 and -27.7‰, only slightly more negative than the $\delta^{13}C_{org}$
721 values of the coastal cliffs, and C/N ratios between 10.1 and 12.6.

722 Both bulk terrigenous proxies thus reflect a strong terrigenous signal in the Yenisei River
723 Mouth, that decreases downstream, and a strong terrigenous signal in the Khalmyer Bay. This reflects
724 the spatial pattern of the BIT index. The good correlation between BIT and the bulk proxies for
725 terrigenous matter in the marine system (r^2 with $\delta^{13}C_{org}$= 0.60, r^2 with C/N = 0.50; after exclusion of
726 one outlier) is in agreement with a recent study performed on the GDGT and bulk organic matter
727 proxies in front of the Kolyma River in the East Siberian Sea, where a similar (albeit exponential)
728 decrease in BIT values was observed with decreasing $\delta^{13}C_{org}$ values (Doğrul Selver et al., 2015). A

729 non-linear relationship between BIT-values and the $\delta^{13}C_{org}$ of bulk organic carbon was also observed
730 by Sparkes et al. (2015), in a study on widely distributed East Siberian Sea sediments. The linear
731 relationship encountered in the Kara Sea sediments indicates that the BIT-index is a robust proxy to
732 trace changes in the input of terrigenous OM in this shallow shelf sea.
733
734 *5.5. Implications for palaeoclimate reconstructions*
735 The reconstruction of palaeotemperature and soil pH, based on marine sedimentary brGDGTs
736 relies on the conservation of a soil-derived brGDGT signal during its transport in the river and in the
737 marine system. This is, however, not the case in the Yenisei River watershed, where in-situ production
738 in the river water and in the marine system influence the brGDGT distributions that are derived from
739 the watershed soils and coastal cliffs. However, preferential degradation of a labile pool of brGDGTs
740 possibly results in a dominantly soil-derived brGDGT signal in offshore sediments. The influence of
741 terrigenous material in these offshore sediments is confirmed by the bulk $\delta^{13}C_{org}$ values and C/N ratios
742 (see section 5.4).
743 The possible impact of the changing distributions on palaeoclimate reconstructions is evident
744 when we reconstruct the pH and MAT. Compared to the Yenisei River SPM (reconstructed pH
745 between 6.9 and 7.9), the reconstructed pH [Eq. 2 and 3] is lower (i.e. 6.5-7.0) in the Yenisei River
746 Mouth (Fig. 7A). This decrease is caused by the strong decrease in fractional abundance of the 6-Me
747 brGDGTs IIa' and IIIa' (Fig. 4). Furthermore, the reconstructed pH decreases further downstream (pH
748 6-7). This is fairly high compared to the soils present in the Yenisei River watershed (average pH = 5;
749 De Jonge et al., 2014a), although some soils fall within this range. As the marine in-situ production of
750 brGDGTs increases the fraction of brGDGTs that are typical for high pH conditions (Fig. 6A; De
751 Jonge et al., 2014b), this may influence the reconstructed pH. For the Khalmyer Bay sediments the
752 brGDGT distributions indicate more acidic conditions (pH 5.5 – 6.0; Fig. 7A), probably reflecting an
753 input dominated by coastal cliffs.
754 Using the MAT_{mr} calibration [Eq. 5], the reconstructed MAT in the Yenisei River Mouth varies
755 between 4 and 5 °C. Fig. 7B shows that the reconstructed temperature increases going downstream. In
756 offshore Yenisei Outflow and Kara Sea sediments, the reconstructed MAT is between 8 and 10°C.

Although the MAT_{mr} is calibrated against the MAT, this value overestimates the measured MAT in the Yenisei River watershed significantly (measured MAT is between -8°C and 1°C, De Jonge et al., 2014a). However, this is to be expected, as high latitude soils have shown a consistent warm offset using all published soil calibrations (Weijers et al., 2007a, Peterse et al., 2012, De Jonge et al., 2014b). These authors postulated that soil bacteria possibly have a lower metabolism and lipid production in under conditions where water in the soil is frozen. Although we expect a large contribution of fossilized brGDGTs in the coastal cliff samples collected at the Yenisei River Mouth (MAT_{mr} between -1 and 8°C, modern measured MAT -11°C), a warm bias in the reconstructed MAT is observed here, but also in the mountainous floodplain and lowland outcrop soil samples (MAT_{mr} 4 and 10 °C, measured MAT between -6 and -6.4 °C, respectively). Following our hypothesis that the majority of brGDGTs in the Kara Sea sediments are derived from watershed soils, our results indicate that the Yenisei watershed soils record a temperature signal that is above the annual average in the Yenisei River catchment, and possibly rather reflect a mean summer temperature (MST measured in the Yenisei River watershed is between 7.5 and 16 °C; De Jonge et al., 2014a). Furthermore, as the precise source region of the least labile brGDGT pools remains unknown, it is possible that the brGDGT distributions and the reconstructed pH and MAT reflect only a part of the Yenisei watershed. This is exemplified by the brGDGT distribution of the soil S_2, with strongly increased fractional abundance of brGDGT Ia. The extent of less labile soil types and the mechanisms behind their conservation are, however, unknown.

6. Conclusions

We have quantified the full suite of 15 brGDGT compounds in the Yenisei River and its outflow in the Kara Sea system. BrGDGTs are present throughout the system, both in the SPM and sediments. The brGDGT distribution in the Yenisei River SPM, with a large abundance of 6-Me brGDGTs, confirms its in-situ production in the river system, as previously assessed by De Jonge et al. (2014a). However, after remaining fairly constant within the Yenisei River, brGDGTs distributions change drastically in the Yenisei Mouth/Kara Sea system. Firstly, a strong decrease in the fractional abundance of the 6-Me brGDGTs IIa' and IIIa' is observed in the Yenisei River Mouth. This offset can be due to

785 the presence of brGDGTs delivered during the freshet, whose distribution can be offset from the signal
786 present in the Yenisei River base flow in September. Also thermoabrasive coastal cliff sediments
787 contain brGDGTs and can influence the brGDGT distribution, especially in sites with no major river
788 input. Further downstream, the fractional abundance of number of minor, cyclopentane containing
789 brGDGTs and brGDGT Ia increases. Marine in-situ production has been invoked to explain changing
790 brGDGT distributions, and is probably the mechanism causing the increase of the pH-sensitive
791 cyclopentane-containing compounds. However, the distribution present in offshore marine Kara Sea
792 sediments is distinct from previously described in-situ produced brGDGT distributions in the Arctic
793 Ocean (Peterse et al., 2012), especially as it has a strongly increased fractional abundance of brGDGT
794 Ia. We postulate that preferential degradation of a modern brGDGT subpool can cause a downstream
795 shift in brGDGT distributions. As the most labile brGDGTs subpool, produced in-situ in the Yenisei
796 River, will be degraded preferentially, this implies that coastal cliff and soil-derived brGDGT lipids
797 possibly dominate the most offshore sediments. Whereas the encountered brGDGT distribution is
798 distinct from the coastal cliffs, it agrees better with a lowland peat. Based on the reconstructed MAT in
799 these sediments, we postulate that the Yenisei watershed soils record a summer temperature. The
800 reconstructed pH is influenced by marine in-situ production.

801 The three invoked terrestrial brGDGT sources (river SPM, watershed soils, coastal cliffs) are
802 characterized by high BIT values. Even though their relative contribution to the marine system is not
803 constrained well, the BIT values are high in both the Yenisei River Mouth and Khalmyer Bay. The
804 decrease in the brGDGTs abundance offshore is reflected by a decrease in the BIT-index. As the BIT-
805 index in the Kara Sea sediments correlates well with bulk OM proxies that trace terrigenous matter,
806 the $\delta^{13}C$ and C/N values, it performs well as a tracer for riverine/terrigenous OM input.

807 The complex behaviour of brGDGTs in the Yenisei River and Kara Sea, indicates that
808 palaeoclimate reconstructions performed on Kara Sea sediment cores will be challenging. We
809 recommend that sediment cores should be collected in offshore Kara Sea sediments, as the distribution
810 closer to the river Mouth is subjected to strong shifts, probably due to preferential degradation.
811 Climatic changes, resulting in changing sea level and discharge patterns, can influence the geographic
812 location of this process, complicating the interpretation of a climatic archive collected in the Yenisei

River Mouth and Gulf. We postulate that modern sediments collected further offshore are dominated by less labile soil-derived brGDGTs. The Kara Sea thus represents a rare situation where the supply of soil-derived brGDGTs is sufficient to dominate a marine in-situ produced signal, after the degradation of 'modern', aquatic brGDGTs. However, the less labile subpool that is represented after the preferential degradation does not necessarily reflect the entire Yenisei watershed. Furthermore, the extent to which this less labile subpool responds to climatic changes is unknown. The downcore behaviour of the brGDGTs distribution in the Kara Sea, and its potential to reconstruct palaeoclimate shifts in the Yenisei watershed thus remains to be investigated.

Thus, palaeoclimate reconstructions performed on Kara Sea sediment cores will have to identify the source of the conserved brGDGT pool, and take the influence of freshwater and marine in-situ production of brGDGTs into account. However, our study does indicate that although brGDGT-based palaeoclimate reconstructions in offshore Kara Sea sediments will be complicated, they are still possible.

7. Acknowledgments

We thank Anchelique Mets for her contribution to the work-up and analysis of the Kara Sea sediments. We thank Dr. R. Smith and an anonymous referee for their helpful comments. This work was performed in the framework of the memorandum NIOZ-VNIIOkeangeologia for Arctic research. The research was funded by research project 819.01.013, financed by the Netherlands Organization for Scientific Research (NWO) and the European Research Council under the EU Seventh Framework Programme (FP7/2007-2013)/ERC grant agreement No. [226600].

8. References

Aagaard K. and Coachman L. K. (1975) Toward an ice-free Arctic ocean. *Eos, Trans. AGU.* **56**, 484–486.

Bendle J. A., Weijers J. W. H., Maslin M. A., Sinninghe Damsté J. S., Schouten S., Hopmans E. C., Boot C. S. and Pancost R. D. (2010) Major changes in glacial and Holocene terrestrial

temperatures and sources of organic carbon recorded in the Amazon fan by tetraether lipids. *Geochem. Geophy. Geosy.* **11**.

Blair N. E. and Aller R. C. (2012) The Fate of Terrestrial Organic Carbon in the Marine Environment. *Ann. Rev. Mar. Sci.* **4**, 401–423.

Bobrovitskaya N. N., Zubkova C. and Meade R. H. (1996) Discharges and yields of suspended sediment in the Ob and Yenisey Rivers of Siberia. In *Erosion and sediment yield: global and regional perspectives. Proceedings of an international symposium, Exeter, 15-19 July 1996* (eds. Walling D. E., Webb B. W. and International Association of Hydrological Sciences), IAHS Press, Wallingford. pp. 115-124.

De Jonge C., Hopmans E. C., Stadnitskaia A., Rijpstra W. I. C., Hofland R., Tegelaar E. and Sinninghe Damsté J. S. (2013) Identification of novel penta- and hexamethylated branched glycerol dialkyl glycerol tetraethers in peat using HPLC–MS^2, GC–MS and GC–SMB-MS. *Org. Geochem.* **54**, 78–82.

De Jonge C., Stadnitskaia A., Hopmans E. C., Cherkashov G., Fedotov A. and Sinninghe Damsté J. S. (2014a) In situ produced branched glycerol dialkyl glycerol tetraethers in suspended particulate matter from the Yenisei River, Eastern Siberia. *Geochim. Cosmochim. Acta* **125**, 476–491.

De Jonge C., Hopmans E. C., Zell C. I., Kim J.-H., Schouten S. and Sinninghe Damsté J. S. (2014b) Occurrence and abundance of 6-methyl branched glycerol dialkyl glycerol tetraethers in soils: Implications for palaeoclimate reconstruction. *Geochim. Cosmochim. Acta* **141**, 97–112

Doğrul Selver A., Sparkes R. B., Bischoff J., Talbot H. M., Gustafsson Ö., Semiletov I. P., Dudarev O. V., Boult S. and van Dongen B. E. (2015) Distributions of bacterial and archaeal membrane lipids in surface sediments reflect differences in input and loss of terrestrial organic carbon along a cross-shelf Arctic transect. *Organic Geochemistry* **83-84**, 16–26.

Donders T. H., Weijers J. W. H., Munsterman D. K., Hoeve M. L. K., Buckles L. K., Pancost R. D., Schouten S., Sinninghe Damsté J. S. and Brinkhuis H. (2009) Strong climate coupling of

865 terrestrial and marine environments in the Miocene of northwest Europe. *Earth Planet. Sci. Lett.*
866 **281**, 215–225.

867 Fernandes M. B. and Sicre M.-A. (2000) The importance of terrestrial organic carbon inputs on Kara
868 Sea shelves as revealed by n-alkanes, OC and $\delta^{13}C$ values. *Org. Geochem.* **31**, 363–374.

869 Gao L., Nie J., Clemens S., Liu W., Sun J., Zech R. and Huang Y. (2012) The importance of solar
870 insolation on the temperature variations for the past 110kyr on the Chinese Loess Plateau.
871 *Palaeogeogr. Palaeoclimatol. Palaeoecol.* **317-318**, 128–133.

872 Gaye B., Fahl K., Kodina L. A., Lahajnar N., Nagel B., Unger D. and Gebhardt A. C. (2007)
873 Particulate matter fluxes in the southern and central Kara Sea compared to sediments: Bulk
874 fluxes, amino acids, stable carbon and nitrogen isotopes, sterols and fatty acids. *Cont. Shelf Res.*
875 **27**, 2570–2594.

876 Hedges J. I. and Keil R. G. (1995) Sedimentary organic matter preservation: an assessment and
877 speculative synthesis. *Mar. Chem.* **49**, 81–115.

878 Hopmans E. C., Weijers J. W. H., Schefuß E., Herfort L., Sinninghe Damsté J. S. and Schouten S.
879 (2004) A novel proxy for terrestrial organic matter in sediments based on branched and isoprenoid
880 tetraether lipids. *Earth Planet. Sci. Lett.* **224**, 107–116.

881 Huguet C., Hopmans E. C., Febo-Ayala W., Thompson D. H., Sinninghe Damsté J. S. and Schouten S.
882 (2006) An improved method to determine the absolute abundance of glycerol dibiphytanyl
883 glycerol tetraether lipids. *Org. Geochem.* **37**, 1036–1041.

884 Huguet C., de Lange G. J., Gustafsson O., Middelburg J. J., Sinninghe Damsté J. S. and Schouten S.
885 (2008) Selective preservation of soil organic matter in oxidized marine sediments (Madeira
886 Abyssal Plain). *Geochim. Cosmochim. Acta* **72**, 6061–6068.

887 Karpov E.G., 1984. About the origin of an underground massive ice within the mouth of the Yenisey
888 River (in Russian) Geologia I Geophisika, 1, pp.1-5.

889 Keil R.G., and Mayer L.M. (2014) Mineral Matrices and Organic Matter. In: Holland H.D. and
890 Turekian K.K. (eds.) *Treatise on Geochemistry*, Second Edition, vol. 12, pp. 337-359. Oxford:
891 Elsevier.

892 Kim J.-H., Schouten S., Buscail R., Ludwig W., Bonnin J., Sinninghe Damsté J. S. and Bourrin F.
893 (2006) Origin and distribution of terrestrial organic matter in the NW Mediterranean (Gulf of
894 Lions): Exploring the newly developed BIT index. *Geochem. Geophy. Geosy.* **7**.

895 Kim J.-H., Zell C., Moreira-Turcq P., Perez M. A. P., Abril G., Mortillaro J.-M., Weijers J. W. H.,
896 Meziane T. and Sinninghe Damsté J. S. (2012) Tracing soil organic carbon in the lower Amazon
897 River and its tributaries using GDGT distributions and bulk organic matter properties. *Geochim.*
898 *Cosmochim. Acta.* **90**, 163–180.

899 Krishnamurthy R. V., Machavaram M., Baskaran M., Brooks J. M. and Champ M. A. (2001) Organic
900 Carbon Flow in the Ob, Yenisey Rivers and Kara Sea of the Arctic Region. *Mar. Pollut. Bull.* **42**,
901 726–732.

902 Lammers R. B., Shiklomanov A. I., Vörösmarty C. J., Fekete B. M. and Peterson B. J. (2001)
903 Assessment of contemporary Arctic river runoff based on observational discharge records. *J.*
904 *Geophys. Res.* **106**, 3321–3334.

905 Lantuit H., Overduin P. P., Couture N., Wetterich S., Aré F., Atkinson D., Brown J., Cherkashov G.,
906 Drozdov D., Forbes D. L., Graves-Gaylord A., Grigoriev M., Hubberten H.-W., Jordan J.,
907 Jorgenson T., Ødegård R. S., Ogorodov S., Pollard W. H., Rachold V., Sedenko S., Solomon S.,
908 Steenhuisen F., Streletskaya I. and Vasiliev A. (2012) The Arctic Coastal Dynamics Database: A
909 New Classification Scheme and Statistics on Arctic Permafrost Coastlines. *Estuaries and Coasts*
910 **35**, 383–400.

911 Lengger S. K., Hopmans E. C., Sinninghe Damsté J. S. and Schouten S. (2014) Fossilization and
912 degradation of archaeal intact polar tetraether lipids in deeply buried marine sediments (Peru
913 Margin). *Geobiology* **12**, 212–220.

914 Lisitsyn A. P. (1995) Marginal Filter of the Ocean. *Oceanology* **34**, 671–682.

915 Lobbes J. M., Fitznar H. P. and Kattner G. (2000) Biogeochemical characteristics of dissolved and
916 particulate organic matter in Russian rivers entering the Arctic Ocean. *Geochim. Cosmochim.*
917 *Acta.* **64**, 2973–2983.

918 Loomis S. E., Russell J. M. and Sinninghe Damsté J. S. (2011) Distributions of branched GDGTs in
919 soils and lake sediments from western Uganda: Implications for a lacustrine paleothermometer.
920 *Org. Geochem.* **42**, 739–751.

921 Loomis S. E., Russell J. M., Heureux A. M., D'Andrea W. J. and Sinninghe Damsté J. S. (2014)
922 Seasonal variability of branched glycerol dialkyl glycerol tetraethers (brGDGTs) in a temperate
923 lake system. *Geochim. Cosmochim. Acta* **144**, 173-187.

924 Michener R. H. and Lajtha K. (2007) Stable isotopes in ecology and environmental science, in:
925 **Ecological Methods and Concepts Series**, Blackwell Pub., Malden, MA.

926 Naidu A. S., Scalan R. S., Feder H. M., Goering J. J., Hameedi M. J., Parker P. L., Behrens E. W.,
927 Caughey M. E. and Jewett S. C. (1993) Stable organic carbon isotopes in sediments of the north
928 Bering-south Chukchi seas, Alaskan-Soviet Arctic Shelf. *Cont. Shelf Res.* **13**, 669–691.

929 Niemann H., Stadnitskaia A., Wirth S. B., Gilli A., Anselmetti F. S., Sinninghe Damsté J. S., Schouten
930 S., Hopmans E. C. and Lehmann M. F. (2012) Bacterial GDGTs in Holocene sediments and
931 catchment soils of a high Alpine lake: application of the MBT/CBT-paleothermometer. *Clim.*
932 *Past.* **8**, 889–906.

933 Pavlov V. K. and Pfirman S. L. (1995) Hydrographic structure and variability of the Kara Sea:
934 Implications for pollutant distribution. *Deep-Sea Res. Pt II.* **42**, 1369–1390.

935 Peterse F., Kim J. H., Schouten S., Kristensen D. K., Koc N. and Sinninghe Damsté J. S. (2009)
936 Constraints on the application of the MBT/CBT palaeothermometer at high latitude environments
937 (Svalbard, Norway). *Org. Geochem.* **40**, 692–699.

938 Peterse F., Nicol G. W., Schouten S. and Sinninghe Damsté J. S. (2010) Influence of soil pH on the
939 abundance and distribution of core and intact polar lipid-derived branched GDGTs in soil. *Org.*
940 *Geochem.* **41**, 1171–1175.

941 Peterse F., Prins M. A., Beets C. J., Troelstra S. R., Zheng H., Gu Z., Schouten S. and Sinninghe
942 Damsté J. S. (2011) Decoupled warming and monsoon precipitation in East Asia over the last
943 deglaciation. *Earth Plan. Sci. Lett.* **301**, 256–264.

944 Peterse F., van der Meer J., Schouten S., Weijers J. W. H., Fierer N., Jackson R. B., Kim J.-H. and
945 Sinninghe Damsté J. S. (2012) Revised calibration of the MBT–CBT paleotemperature proxy
946 based on branched tetraether membrane lipids in surface soils. *Geochim. Cosmochim. Acta.* **96**,
947 215–229.

948 Peterse F., Martínez-García A., Zhou B., Beets C. J., Prins M. A., Zheng H. and Eglinton T. I. (2014a)
949 Molecular records of continental air temperature and monsoon precipitation variability in East
950 Asia spanning the past 130,000 years. *Quaternary Sci. Rev.* **83**, 76–82.

951 Peterse F., Vonk J. E., Holmes R. M., Giosan L., Zimov N. and Eglinton T. I. (2014b) Branched
952 glycerol dialkyl glycerol tetraethers in Arctic lake sediments: Sources and implications for
953 paleothermometry at high latitudes: Branched GDGTs in Arctic lakes. *J. Geophys. Res.- Biogeo.*
954 **119**, 1738-1754.

955 Pitcher A., Hopmans E. C., Schouten S. and Sinninghe Damsté J. S. (2009) Separation of core and
956 intact polar archaeal tetraether lipids using silica columns: Insights into living and fossil biomass
957 contributions. *Org. Geochem.* **40**, 12–19.

958 Polyak L., Levitan M., Gataullin V., Khusid T., Mikhailov V. and Mukhina V. (2000) The impact of
959 glaciation, river-discharge and sea-level change on Late Quaternary environments in the
960 southwestern Kara Sea. *Int. J. Earth Sci.* **89**, 550–562.

961 Pross J., Contreras L., Bijl P. K., Greenwood D. R., Bohaty S. M., Schouten S., Bendle J. A., Röhl U.,
962 Tauxe L., Raine J. I., Huck C. E., Van De Flierdt T., Jamieson S. S. R., Stickley C. E., Van De
963 Schootbrugge B., Escutia C., Brinkhuis H., Dotti C. E., Klaus A., Fehr A., Williams T., Bendle J.
964 A. P., Carr S. A., Dunbar R. B., Gonzàlez J. J., Hayden T. G., Iwai M., Jimenez-Espejo F. J.,
965 Katsuki K., Soo Kong G., Mckay R. M., Nakai M., Olney M. P., Passchier S., Pekar S. F.,
966 Riesselman C. R., Sakai T., Shrivastava P. K., Sugisaki S., Tuo S., Welsh K. and Yamane M.

(2012) Persistent near-tropical warmth on the Antarctic continent during the early Eocene epoch. *Nature* **487**, 73–77.

Schouten S., Hopmans E. C., Pancost R. D. and Sinninghe Damsté J. S. (2000) Widespread occurrence of structurally diverse tetraether membrane lipids: Evidence for the ubiquitous presence of low-temperature relatives of hyperthermophiles. *PNAS* **97**, 14421–14426.

Schouten S., Huguet C., Hopmans E. C., Kienhuis M. V. M. and Sinninghe Damsté J. S. (2007) Analytical Methodology for TEX_{86} Paleothermometry by High-Performance Liquid Chromatography/Atmospheric Pressure Chemical Ionization-Mass Spectrometry. *Anal. Chem.* **79**, 2940–2944.

Schouten S., Eldrett J., Greenwood D. R., Harding I., Baas M. and Sinninghe Damsté J. S. (2008) Onset of long-term cooling of Greenland near the Eocene-Oligocene boundary as revealed by branched tetraether lipids. *Geol.* **36**, 147–150.

Schouten S., Hopmans E. C., Rosell-Melé A., Pearson A., Adam P., Bauersachs T., Bard E., Bernasconi S. M., Bianchi T. S., Brocks J. J., Carlson L. T., Castañeda I. S., Derenne S., Selver A. D., Dutta K., Eglinton T., Fosse C., Galy V., Grice K., Hinrichs K.-U., Huang Y., Huguet A., Huguet C., Hurley S., Ingalls A., Jia G., Keely B., Knappy C., Kondo M., Krishnan S., Lincoln S., Lipp J., Mangelsdorf K., Martínez-García A., Ménot G., Mets A., Mollenhauer G., Ohkouchi N., Ossebaar J., Pagani M., Pancost R. D., Pearson E. J., Peterse F., Reichart G.-J., Schaeffer P., Schmitt G., Schwark L., Shah S. R., Smith R. W., Smittenberg R. H., Summons R. E., Takano Y., Talbot H. M., Taylor K. W. R., Tarozo R., Uchida M., van Dongen B. E., Van Mooy B. A. S., Wang J., Warren C., Weijers J. W. H., Werne J. P., Woltering M., Xie S., Yamamoto M., Yang H., Zhang C. L., Zhang Y., Zhao M. and Sinninghe Damsté J. S. (2013a) An interlaboratory study of TEX_{86} and BIT analysis of sediments, extracts, and standard mixtures. *Geochem. Geophys. Geosyst.* **14**, 5263–5285.

Schouten S., Hopmans E. C. and Sinninghe Damsté J. S. (2013b) The organic geochemistry of glycerol dialkyl glycerol tetraether lipids: A review. *Org. Geochem.* **54**, 19–61.

993 Shpolyanskaya N. A. (2003) Massive ground ice as a basis for paleogeographic reconstruction. In:
994 *Permafrost: proceedings of the 8th International Conference on Permafrost, Zurich, Switzerland,*
995 *21-25 July 2003*. eds. M. Phillips, S. M. Springman, and L. U. Arenson, A.A. Balkema
996 Publishers, Lisse [Netherlands] ; Exton, PA.

997 Sinninghe Damsté J. S., Hopmans E. C., Pancost R. D., Schouten S. and Geenevasen J. a. J. (2000)
998 Newly discovered non-isoprenoid glycerol dialkyl glycerol tetraether lipids in sediments. *Chem.*
999 *Commun.* **17**, 1683–1684.

1000 Sinninghe Damsté, J. S., Schouten S., Hopmans E. C., van Duin A. C. T. and Geenevasen J. A. J.
1001 (2002) Crenarchaeol: the characteristic core glycerol dibiphytanyl glycerol tetraether membrane
1002 lipid of cosmopolitan pelagic crenarchaeota. *J. Lipid Res.* **43**, 1641–1651.

1003 Sinninghe Damsté J. S., Ossebaar J., Abbas B., Schouten S. and Verschuren D. (2009) Fluxes and
1004 distribution of tetraether lipids in an equatorial African lake: Constraints on the application of the
1005 TEX_{86} palaeothermometer and BIT index in lacustrine settings. *Geochim. Cosmochim. Acta.* **73**,
1006 4232–4249.

1007 Sinninghe Damsté J. S., Rijpstra W. I. C., Hopmans E. C., Weijers J. W. H., Foesel B. U., Overmann J.
1008 and Dedysh S. N. (2011) 13, 16-dimethyl octacosanedioic acid (iso-diabolic acid), a common
1009 membrane-spanning lipid of Acidobacteria subdivisions 1 and 3. *Appl. Environ. Microb.* **77**,
1010 4147–4154.

1011 Sinninghe Damsté J. S., Ossebaar J., Schouten S. and Verschuren D. (2012) Distribution of tetraether
1012 lipids in the 25-ka sedimentary record of Lake Challa: Extracting reliable TEX_{86} and MBT/CBT
1013 palaeotemperatures from an equatorial African lake. *Quat. Sci. Rev.* **50**, 43–54.

1014 Smith R. W., Bianchi T. S. and Li X. (2012) A re-evaluation of the use of branched GDGTs as
1015 terrestrial biomarkers: Implications for the BIT Index. *Geochim. Cosmochim. Acta* **80**, 14–29.

1016 Sparkes R. B., Doğrul Selver A., Bischoff J., Talbot H. M., Gustafsson ö., Semiletov I. P., Dudarev O.
1017 V. and van Dongen B. E. (2015) GDGT distributions in the East Siberian Sea: implications for
1018 organic carbon export, burial and degradation. *Biogeosciences Discussions* **12**, 637–674.

Streletskaya I. D., Vasiliev A. A. and Vanstein B. G. (2009) Erosion of Sediment and Organic Carbon from the Kara Sea Coast. *AAAR* **41**, 79–87.

Telang S. A., Pocklington R., Naidu A. S., Romankevich E. A., Gitelson I. I. and Gladyshev M. I. (1990) Carbon and mineral transport in major North American, Russian, and Siberian rivers: the St Lawrence, the Mackenzie, the Yukon, the Arctic Alaskan rivers, the Arctic Basin rivers, and the Yenisei. In *Biogeochemistry of Major World Rivers SCOPE*. John Wiley & sons. pp. 75–104.

Tierney J. E. and Russell J. M. (2009) Distributions of branched GDGTs in a tropical lake system: Implications for lacustrine application of the MBT/CBT paleoproxy. *Org. Geochem.* **40**, 1032–1036.

Tyler J. J., Nederbragt A. J., Jones V. J. and Thurow J. W. (2010) Assessing past temperature and soil pH estimates from bacterial tetraether membrane lipids: Evidence from the recent lake sediments of Lochnagar, Scotland. *J. Geophys. Res.* **115**.

Vonk J. E., Sánchez-García L., Semiletov I., Dudarev O., Eglinton T., Andersson A. and Gustafsson O. (2010) Molecular and radiocarbon constraints on sources and degradation of terrestrial organic carbon along the Kolyma paleoriver transect, East Siberian Sea. *Biogeosciences* **7**, 3153–3166.

Weijers J. W. H., Schouten S., Hopmans E. C., Geenevasen J. A. J., David O. R. P., Coleman J. M., Pancost R. D. and Sinninghe Damsté J. S. (2006) Membrane lipids of mesophilic anaerobic bacteria thriving in peats have typical archaeal traits. *Environ. Microbiol.* **8**, 648–657.

Weijers J. W. H., Schouten S., van den Donker J. C., Hopmans E. C. and Sinninghe Damsté J. S. (2007a) Environmental controls on bacterial tetraether membrane lipid distribution in soils. *Geochim. Cosmochim. Acta.* **71**, 703–713.

Weijers J. W. H., Schefuss E., Schouten S. and Sinninghe Damsté J. S. (2007b) Coupled Thermal and Hydrological Evolution of Tropical Africa over the Last Deglaciation. *Science* **315**, 1701–1704.

1043 Weijers J. W. H., Schouten S., Sluijs A., Brinkhuis H. and Sinninghe Damsté J. S. (2007c) Warm arctic
1044 continents during the Palaeocene–Eocene thermal maximum. *Earth Planet. Sci. Lett.* **261**, 230–
1045 238.

1046 Weijers J. W. H., Panoto E., van Bleijswijk J., Schouten S., Rijpstra W. I. C., Balk M., Stams A. J. M.
1047 and Sinninghe Damste J. S. (2009) Constraints on the Biological Source(s) of the Orphan
1048 Branched Tetraether Membrane Lipids. *Geomicrobiol. J.* **26**, 402–414.

1049 White D. C., Davis W. M., Nickels J. S., King J. D. and Bobbie R. J. (1979) Determination of the
1050 sedimentary microbial biomass by extractible lipid phosphate. *Oecologia* **40**, 51–62.

1051 Yang H., Ding W., Zhang C. L., Wu X., Ma X., He G., Huang J. and Xie S. (2011) Occurrence of
1052 tetraether lipids in stalagmites: Implications for sources and GDGT-based proxies. *Org. Geochem.*
1053 **42**, 108–115.

1054 Yang G., Zhang C. L., Xie S., Chen Z., Gao M., Ge Z. and Yang Z. (2013) Microbial glycerol dialkyl
1055 glycerol tetraethers from river water and soil near the Three Gorges Dam on the Yangtze River.
1056 *Org. Geochem.* **56**, 40–50.

1057 Zell C., Kim J.-H., Moreira-Turcq P., Abril G., Hopmans E. C., Bonnet M.-P., Sobrinho R. L. and
1058 Sinninghe Damsté J. S. (2013) Disentangling the origins of branched tetraether lipids and
1059 crenarchaeol in the lower Amazon river: Implications for GDGT-based proxies. *Limnol.*
1060 *Oceanogr.* **58**, 343–353.

1061 Zell C., Kim J.-H., Balsinha M., Dorhout D., Fernandes C., Baas M. and Sinninghe Damsté J. S.
1062 (2014a) Transport of branched tetraether lipids from the Tagus River basin to the coastal ocean of
1063 the Portuguese margin: consequences for the interpretation of the MBT'/CBT paleothermometer.
1064 *Biogeosciences* **11**, 5637–5655.

1065 Zell C., Kim J.-H., Hollander D., Lorenzoni L., Baker P., Silva C. G., Nittrouer C. and Sinninghe
1066 Damsté J. S. (2014b) Sources and distributions of branched and isoprenoid tetraether lipids on the
1067 Amazon shelf and fan: implications for the use of GDGT-based proxies in marine sediments.
1068 *Geochim. Cosmochim. Acta.* **139**, 293-312.

1069 Zhang C. L., Wang J., Wei Y., Zhu C., Huang L. and Dong H. (2012) Production of Branched
1070 Tetraether Lipids in the Lower Pearl River and Estuary: Effects of Extraction Methods and Impact
1071 on bGDGT Proxies. *Front. Microbiol.* **2**. 274.

1072 Zhu C., Weijers J. W. H., Wagner T., Pan J. M., Chen J. F. and Pancost R. D. (2011) Sources and
1073 distributions of tetraether lipids in surface sediments across a large river-dominated continental
1074 margin. *Org. Geochem.* **42**, 376–386.
1075

Figure captions

Fig. 1. Chemical structures of branched GDGTs (I-III) and crenarchaeol (IV). The chemical structures of the hexa- and pentamethylated brGDGTs with cyclopentyl moiety(ies) IIb', IIc', IIIb' and IIIc' are tentatively assigned.

Fig. 2. A) Satellite image of the Ob River Mouth, the Khalmyer Bay and Yenisei River Mouth, showing the increase in sediment load in the Khalmyer Bay and Yenisei Gulf that can be related to coastal cliff erosion. NASA image courtesy Norman Kuring, Ocean Color Web. B) Overview map of the Yenisei River, with sample sites indicated. Red asterisks indicate sites of watershed soil samples. C) Map of the Kara Sea, with sampling locations and Yenisei and Ob River Mouths and Khalmyer Bay indicated. Red asterisks indicate sampling sites of coastal cliff samples. In panel B) and C) symbol colours divide the stations in geographical zones, as reflected by the legend.

Fig. 3. A-B) Core lipid BIT values in suspended particulate matter (SPM; A) and sediments (B). Colours of the dots refer to the BIT-colour scale indicated. C-D) BIT values plotted vs. GDGT concentration, with brGDGTs plotted as closed symbols and crenarchaeol as open symbols, in both the SPM (C panel) and sediments (D panel). E-F) Sedimentary BIT-values plotted versus the sedimentary $\delta^{13}C_{org}$ values (E) and C/N ratio (F).

Fig. 4. Bar plots of the fractional abundance of brGDGTs in the CL (A-D and H-K) and IPL (E-G and L-O) fractions of the SPM (A-G) and sediments (H-O), respectively. The fractional abundances are averaged per geographical zone, as defined in Table 1. For the CL fraction, the average score on the first three PC is reported per geographical zone. For clarity, brGDGTs with a large standard deviation (sd) of their fractional abundance (reflecting the variance within the geographical zone) only have the lower halve of the range (range = 2 x sd) plotted. The colour of the bars refer to the brGDGT structure, as reflected in the figure legend. As only samples with >8 brGDGTs quantified were plotted, the number of observations per zone is reported, and zones without any samples with >8 compounds, have no corresponding bar plot.

1104

1105 Fig. 5. Bar plots of the fractional abundance of brGDGTs in the CL (A, B, D) and IPL (C) fractions of
1106 the Khalmyer Bay and Gulf sediments (A, C) and SPM (B). Furthermore, a number of possible
1107 sources of brGDGTs is reported, being the coastal cliffs (D), a mountainous peat sample from the
1108 floodplain of a lake (E) and a lowland peat sampled at 2m depth (F). The fractional abundances are
1109 averaged for the Khalmyer Bay and Gulf (as defined in Table 1) combined. The number of
1110 observations per zone is reported, and to capture the variace between the samples in each dataset, the
1111 range indicated with the whiskers equals 2 x standard deviation. For the CL fraction, the average score
1112 on the first three PC is reported. The colour of the bars refer to the brGDGT structure, as reflected in
1113 the figure legend.

1114

1115 Fig. 6. Biplots of the principal components (PC) based on the fractional abundance of CL brGDGTs,
1116 for those samples that have more than 8 (out of 15) brGDGTs quantified. The first two (A, B) and first
1117 and third PC (C, D) are plotted, representing respectively 37, 29 and 13% of the variance. The
1118 loadings of the variables (A, C) and the scores of the sites (B, D) are plotted. The score of each station
1119 is calculated using the relative abundance of each compound per station and its loading on the PC.
1120 Round symbols indicate SPM brGDGT distributions, rectangles indicate sedimentary brGDGT
1121 distributions, asterisks indicate coastal cliff samples and triangles indicate watershed soil samples. The
1122 colour of the symbols reflects the geographical zone of the station. The red coloured asterisk gives the
1123 score of the weighed average of the coastal cliff brGDGT distributions (n=12). E-G) Plots of the score
1124 on the PC1-3. In subplots a and b the scores are plotted against the straight distance from the river
1125 Mouth (83°17.0383 N, 70°99.675 E), where subplot a has a different scale compared to subplot b. The
1126 4 Kara Sea samples are plotted in subplot c, as the distance from the river Mouth will be a poor
1127 comparison for the length of the flowpath for these samples.

1128

1129 Fig. 7. A) Reconstructed pH [Eq. 3 and 4] and B) reconstructed MAT [Eq. 5], based on the brGDGT
1130 distribution in surface sediments.

Tables

Table 1. Information on the sampled stations. The type of sample, either suspended particulate matter (SPM), sediment, coastal cliff or watershed soil sample is indicated. The coordinates and date of sampling are reported. The depth below sea level (bsl) at which the sample was taken is indicated, both for SPM and sediment samples. N.d. indicates 'not determined', while n.a. indicates 'not applicable'.

Sample code	Zone	Type	Latitude (°N)	Longitude (°E)	Date sampled	Depth bsl (m)
MR1	Mountain River	SPM	54.85631	99.12047	30-6-2010	0.5
MR2	Mountain River	SPM	51.94533	100.78839	11-7-2010	0.5
SR1	Yenisei River	SPM	51.72828	107.46281	6-7-2010	0.5
YR1	Yenisei River	SPM	58.00992	93.11680	25-8-2009	2.0
YR2	Yenisei River	SPM	58.13147	92.75405	29-9-2009	3.0
YR3	Yenisei River	SPM	61.46000	90.08773	27-8-2009	7.0
YR4	Yenisei River	SPM	61.79185	89.54925	25-9-2009	4.0
YR5	Yenisei River	SPM	65.32055	87.95368	29-8-2009	5.0
YR6	Yenisei River	SPM	66.17182	87.23333	20-9-2009	4.5
YR7	Yenisei River	SPM	66.59222	86.57790	31-8-2009	5.0
YR8	Yenisei River	SPM	68.67943	86.26707	1-9-2009	7.0
YR9	Yenisei River	SPM	69.70503	84.20855	3-9-2009	5.0
YM1	Yenisei River Mouth	SPM	70.86107	83.42537	20-9-2009	6.0
YM2	Yenisei River Mouth	SPM	71.87552	82.82212	18-9-2009	4.0
		Sediment				9.5
YM3	Yenisei River Mouth	SPM	71.84173	82.78483	18-9-2009	10.0
		Sediment				23.5
YM4	Yenisei River Mouth	SPM	71.81020	82.74788	19-9-2009	4.5
		Sediment				8.5
YM5	Yenisei River Mouth	SPM	71.76715	82.70532	19-9-2009	3.5
YG1	Yenisei Gulf	SPM	72.64740	80.13693	9-9-2014	7.0
		Sediment				17.0
YG2a	Yenisei Gulf	SPM	73.08272	79.98005	7-9-2009	3.0
YG2b		SPM				15.0
		Sediment				15.0
YG3	Yenisei Gulf	SPM	73.15012	80.49095	6-9-2009	3.0
		Sediment				n.d.
YG4	Yenisei Gulf	SPM	73.36032	80.49095	5-9-2009	3.0
YG5	Yenisei Gulf	SPM	73.40058	80.47580	5-9-2009	5.0

YG6	Yenisei Gulf	SPM	72.71858	79.11492	17-9-2009	1.0
YG7	Yenisei Gulf	SPM	72.55642	79.30307	17-9-2009	5.0
		Sediment				13.5
YG8	Yenisei Gulf	SPM	72.45150	77.05383	15-9-2009	2.0
		Sediment				4.1
YG9	Yenisei Gulf	SPM	72.61993	77.52445	16-9-2009	2.0
		Sediment				5.8
YO1	Yenisei Outflow	SPM	74.28794	78.62166	09-2012	Surface
		Sediment				28
YO2	Yenisei Outflow	SPM	75.68333	83.20000	09-2012	Surface
		Sediment				52
YO3	Yenisei Outflow	SPM	76.08627	84.86278	09-2012	Surface
		Sediment				51
KS1	Kara Sea	SPM	77.21723	78.09048	09-2012	Surface
		Sediment				126
KS2	Kara Sea	SPM	75.83585	68.91351	09-2012	Surface
		Sediment				320
KS3	Kara Sea	SPM	72.33722	65.98106	09-2012	Surface
		Sediment				139
KS4	Kara Sea	SPM	78.48321	72.79748	09-2012	Surface
		Sediment				476
KB1	Khalmyer Bay	SPM	71.17518	77.37713	12-9-2009	1.0
		Sediment				2.0
KB2	Khalmyer Bay	SPM	71.19288	77.45945	13-9-2009	2.0
		Sediment				4.0
KB3	Khalmyer Bay	SPM	71.22395	77.56670	13-9-2009	4.0
		Sediment				7.1
KB4	Khalmyer Bay	SPM	71.24463	77.68583	14-9-2009	2.0
		Sediment				4.5
KG1	Khalmyer Gulf	SPM	71.77597	75.80948	10-9-2009	3.0
		Sediment				10.5
KG2	Khalmyer Gulf	SPM	71.77742	75.97872	11-9-2009	3.0
		Sediment				6.5
OO1	Ob Outflow	SPM	73.56237	73.30226	09-2012	Surface
		Sediment				25
OO2	Ob Outflow	SPM	73.84178	75.09213	09-2012	Surface

		Sediment				22
S_1	Watershed soil	Soil	51.96166	100.95583	11-7-2010	n.a.
S_2	Watershed soil	Soil	66.35770	86.34261	26-8-2009	n.a.
CC_YM1	Coastal Cliff Zone 1	Coastal cliffs	71.22225	83.17480	09-2009	n.a.
CC_YM2	Coastal Cliff Zone 1	Coastal cliffs	71.22225	83.17480	09-2009	n.a.
CC_YM3	Coastal Cliff Zone 1	Coastal cliffs	71.22225	83.17480	09-2009	n.a.
CC_YM4	Coastal Cliff Zone 1	Coastal cliffs	71.22225	83.17480	09-2009	n.a.
CC_YM5	Coastal Cliff Zone 2	Coastal cliffs	71.40538	83.39623	09-2009	n.a.
CC_YM6	Coastal Cliff Zone 2	Coastal cliffs	71.40538	83.39623	09-2009	n.a.
CC_YM7	Coastal Cliff Zone 3	Coastal cliffs	71.88668	82.67953	09-2009	n.a.
CC_YM8	Coastal Cliff Zone 3	Coastal cliffs	71.88668	82.67953	09-2009	n.a.
CC_YM9	Coastal Cliff Zone 3	Coastal cliffs	71.88668	82.67953	09-2009	n.a.
CC_YG1	Coastal Cliff Zone 4	Coastal cliffs	73.51950	80.56168	09-2009	n.a.
CC_YG2	Coastal Cliff Zone 4	Coastal cliffs	73.51950	80.56168	09-2009	n.a.
CC_YG3	CC_YG3	Coastal cliffs	72.72285	79.13363	09-2009	n.a.

1136

1137 Table 2. Summarizes the particulate organic carbon content (POC; $mg.L^{-1}$) and the stable carbon isotope signal
1138 ($\delta^{13}C$) of the SPM samples. B.d.l. indicates that the amounts measured were too low to allow the calculation of
1139 the stable carbon isotope signal.

Sample site	POC ($mg.L^{-1}$)[1]	$\delta^{13}C$ (‰)
MR1	1.6	-28.8
MR2	0.1	-27.8
SR1	6.4	-27.6
YR1	0.03	b.d.l.
YR2	0.09	-30.5
YR3	0.2	-29.3
YR4	0.03	b.d.l.
YR5	0.1	-29.0
YR6	0.4	-31.4
YR7	0.2	-31.3
YR8	0.07	-33.3
YR9	0.1	-35.0
YM1	0.1	-32.6
YM2	0.03	b.d.l.
YM3	0.08	-30.2
YM4	0.6	-28.8
YM5	0.1	-29.6
YG1	0.04	b.d.l.
YG2a	0.02	b.d.l.
YG2b	0.05	b.d.l.
YG3	0.1	b.d.l.
YG4	0.03	-31.9
YG5	0.04	b.d.l.
YG6	8.1	-28.7
YG7	1.2	-28.1
YG8	2.7	-29.0
YG9	2.0	-29.4
YO1	0.06	b.d.l.
YO2	0.09	b.d.l.
YO3	0.06	b.d.l.
KS1	0.08	b.d.l.

KS2	0.1	b.d.l.
KS3	0.1	b.d.l.
KS4	0.1	b.d.l.
KB1	0.2	-29.6
KB2	0.2	-30.0
KB3	0.1	b.d.l.
KB4	1.5	-29.0
KG1	0.1	b.d.l.
KG2	0.3	-29.1
OO1	0.1	b.d.l.
OO2	0.1	b.d.l.

1140

Table 3. Summarizes the total organic carbon content percentage (TOC, % dry weight), the stable carbon isotope signal ($\delta^{13}C$, ‰), the total nitrogen content (TN, % dry weight) and the stable nitrogen isotope signal ($\delta^{15}N$, ‰) of the sediments, coastal cliff and soil samples. N.d. indicates values that were not determined.

Sample site	TOC (%)[1]	$\delta^{13}C$ (‰)	TN (%)[1]	$\delta^{15}N$ (‰)
YM2	0.2	-25.7	0.02	3.7
YM3	0.4	-27.5	0.03	3.6
YM4	1.6	-29.1	0.1	2.7
YG1	2.5	-27.5	0.2	4.3
YG2	2.3	-27.5	0.2	5.1
YG3	2.2	-27.3	0.2	4.6
YG7	2.4	-27.4	0.2	3.9
YG8	0.4	-27.0	0.04	4.1
YG9	0.03	-26.2	0.01	5.2
YO1	1.8	-27.0	0.2	6.2
YO2	1.3	-24.8	0.2	7.3
YO3	1.2	-25.1	0.1	7.2
KS1	0.6	-24.9	0.06	7.3
KS2	1.0	-24.0	0.1	7.9
KS3	1.4	-23.9	0.2	7.8
KS4	1.4	-23.1	0.2	6.2
KB1	0.4	-27.7	0.03	2.4
KB2	0.9	-27.6	0.07	2.4
KB3	0.9	-27.0	0.09	3.1
KB4	0.7	-27.4	0.05	2.3
KG1	0.8	-27.1	0.08	4.1
KG2	0.7	-27.0	0.09	4.1
OO1	1.1	-27.3	0.1	6.5
OO2	0.3	-28.0	0.03	5.9
S_1	n.d.	n.d.	n.d.	n.d.
S_2	48	-26.4	1.0	-1.0
CC_YM1	0.7	-25.2	0.1	3.4
CC_YM2	14	-27.2	0.04	1.0
CC_YM3	0.4	-25.7	0.02	3.6
CC_YM4	1.9	-26.6	0.1	3.0
CC_YM5	n.d.	n.d.	n.d.	n.d.

CC_YM6	10	-24.4	0.2	2.5
CC_YM7	n.d.	n.d.	n.d.	n.d.
CC_YM8	0.8	-26.2	0.1	2.8
CC_YM9	1.0	-26.2	0.1	2.5
CC_YG1	1.8	-27.2	0.2	4.7
CC_YG2	1.4	-26.7	0.1	7.1
CC_YG3	0.9	-26.4	0.1	2.4

1144

Table 4. Summarizes the fractional abundances of the brGDGT compounds of the core lipid (CL) and intact polar lipid (IPL) fractions in the SPM. The amounts of CL brGDGTs and crenarchaeol at each station are reported normalized per gram POC, while the IPL abundances are expressed as the percentage of IPLs relative to the total amount of brGDGTs per site. The calculated BIT index for the IPL and CL fractions [Eq. 2] and the reconstructed MAT [Eq. 5] and pH [Eq. 3 and 4] for the CL fraction are reported. B.d.l. indicates that the amounts measured were below detection limit.

Sample	Fraction	Ia	Ib	Ic	IIa	IIb	IIc	IIIa	IIIb	IIIc	IIa'	IIb'	IIc'	IIIa'	IIIb'	IIIc'	Σ brGDGTs (µg. g POC^{-1}) IPL (%)	crenarchaeol (µg. g POC^{-1}) IPL (%)	BIT	MAT (°C)	pH
MR1	CL	15	2	0.5	21	2	0.3	21	0.3	b.d.l.	14	2	0.1	22	0.5	b.d.l.	1	0.02	0.98	4.5	6.9
	IPL	15	2	0.7	22	2	1	18	b.d.l.	b.d.l.	13	2	1	24	b.d.l.	b.d.l.	11%	58%	0.85		
MR2	CL	11	2	0.4	22	2	0.4	24	0.3	b.d.l.	15	2	0.3	20	1	b.d.l.	15	0.08	0.99	3.5	6.9
	IPL	b.d.l.	b.d.l.	b.d.l.	b.d.l.	b.d.l.	b.d.l.	49	b.d.l.	b.d.l.	7	b.d.l.	b.d.l.	44	b.d.l.	b.d.l.	1%	45%	0.73		
SR1	CL	12	5	0.7	12	4	0.3	8	0.4	b.d.l.	24	7	0.4	24	1	b.d.l.	4	0.2	0.93	7.3	7.5
	IPL	b.d.l.	b.d.l.	b.d.l.	14	4	1	15	2	b.d.l.	17	0.1	1	41	4	b.d.l.	2%	61%	0.17		
YR1	CL	14	3	1	13	2	b.d.l.	9	0.4	0.1	18	3	b.d.l.	36	1	0.1	10	0.3	0.97	6.8	7.5
	IPL	14	3	1	11	2	b.d.l.	8	0.2	b.d.l.	18	2	b.d.l.	40	0.1	b.d.l.	16%	37%	0.91		
YR2	CL	9	3	0.4	9	2	0.2	7	0.4	0.1	19	7	0.2	42	2	0.4	21	0.2	0.99	7.1	7.9
	IPL	b.d.l.	2	0.3	5	1	1	10	1	b.d.l.	12	b.d.l.	1	62	5	b.d.l.	3%	39%	0.83		
YR3	CL	14	2	0.4	12	1	0.2	8	0.4	0.1	20	5	0.2	35	1	0.2	11	0.2	0.98	6.7	7.6
	IPL	13	2	0.3	10	1	0.4	6	0.1	b.d.l.	21	5	0.4	39	1	b.d.l.	13%	37%	0.94		
YR4	CL	14	2	b.d.l.	11	2	b.d.l.	9	b.d.l.	b.d.l.	19	4	b.d.l.	39	b.d.l.	b.d.l.	3	0.06	0.98	6.8	7.6
	IPL	b.d.l.	b.d.l.	b.d.l.	b.d.l.	b.d.l.	b.d.l.	b.d.l.	b.d.l.	b.d.l.	b.d.l.	b.d.l.	b.d.l.	b.d.l.	b.d.l.	b.d.l.	b.d.l.	38%	n.d.		
YR5	CL	14	3	0	12	2	0.3	9	0.4	0.1	20	6	0.2	32	2	0.3	16	0.2	0.99	7	7.5
	IPL	13	3	1	10	2	0.5	7	0.4	b.d.l.	21	6	1	35	2	b.d.l.	10%	40%	0.93		
YR6	CL	11	3	0.5	10	2	0.3	8	1	0.1	18	6	0.2	37	2	0.3	14	0.2	0.99	7	7.7

	IPL	7	2	0.3	8	2	1	9	1	b.d.l.	18	5	1	43	2	b.d.l.	5%	32%	0.88		
YR7	CL	13	2	0.2	10	1	0.2	8	0.4	0.04	21	5	0.2	37	1	0.2	15	0.1	0.99	7	7.7
	IPL	14	0	0.1	11	1	b.d.l.	9	0.4	b.d.l.	18	4	b.d.l.	41	1	b.d.l.	5%	41%	0.88		
YR8	CL	16	2	1	16	2	0.3	11	1	0.1	18	4	0.2	28	1	0.2	12	0.1	0.99	5.9	7.3
	IPL	13	b.d.l.	1	18	2	b.d.l.	14	b.d.l.	b.d.l.	16	2	b.d.l.	33	b.d.l.	b.d.l.	4%	28%	0.91		
YR9	CL	16	2	1	17	2	b.d.l.	12	1	0.1	18	4	b.d.l.	27	1	0.2	9	0.1	0.99	5.9	7.2
	IPL	11	2	1	14	2	b.d.l.	17	b.d.l.	b.d.l.	18	4	b.d.l.	32	b.d.l.	b.d.l.	4%	91%	0.27		
YM1	CL	15	3	0.5	23	2	0.3	21	0.5	0.1	14	3	0.1	17	1	0.2	16	0.2	0.98	4.2	6.8
	IPL	6	3	1.1	23	2	2	29	1	b.d.l.	10	2	1	19	2	b.d.l.	5%	43%	0.81		
YM2	CL	19	3	0.7	23	3	0.5	20	1	0.1	13	3	0.2	15	1	0.2	39	1	0.97	4.8	6.7
	IPL	b.d.l.	b.d.l.	b.d.l.	b.d.l.	b.d.l.	b.d.l.	b.d.l.	b.d.l.	b.d.l.	b.d.l.	b.d.l.	b.d.l.	b.d.l.	b.d.l.	b.d.l.	b.d.l.	38%	n.d.		
YM3	CL	18	3	0.6	22	2	0.4	20	0.5	0.1	14	3	0.2	15	1	0.2	35	1	0.97	4.8	6.7
	IPL	b.d.l.	b.d.l.	b.d.l.	b.d.l.	b.d.l.	b.d.l.	b.d.l.	b.d.l.	b.d.l.	b.d.l.	b.d.l.	b.d.l.	b.d.l.	b.d.l.	b.d.l.	b.d.l.	36%	n.d.		
YM4	CL	17	3	0.6	23	3	0.4	22	0.5	0.1	13	3	0.2	15	1	0.1	27	1	0.97	4.4	6.7
	IPL	b.d.l.	b.d.l.	b.d.l.	4	b.d.l.	1	65	5	b.d.l.	b.d.l.	b.d.l.	b.d.l.	23	2	b.d.l.	0%	41%	0.05		
YM5	CL	17	3	0.6	23	3	0.5	23	0.5	0.1	13	3	0.2	14	1	0.1	34	1	0.97	4.5	6.7
	IPL	b.d.l.	2	1.2	20	b.d.l.	b.d.l.	41	4	b.d.l.	7	b.d.l.	b.d.l.	20	5	b.d.l.	2%	41%	0.5		
YG1	CL	22	3	1	26	3	0.4	19	0.5	0.1	11	2	0.3	11	1	0.1	35	11	0.75	4.4	6.5
	IPL	b.d.l.	b.d.l.	b.d.l.	b.d.l.	b.d.l.	b.d.l.	70	12	b.d.l.	b.d.l.	b.d.l.	b.d.l.	17	1	b.d.l.	0%	37%	n.d.		
YG2a	CL	23	2	1	29	2	0.3	20	0.4	0.1	10	2	0.2	10	0.4	0.1	18	3	0.84	3.6	6.4
	IPL	b.d.l.	3	b.d.l.	30	3	b.d.l.	38	b.d.l.	b.d.l.	8	1	b.d.l.	17	b.d.l.	b.d.l.	2%	26%	0.26		
YG2b	CL	26	3	1	26	3	0.3	17	0.4	0.1	11	2	0.4	9	0.5	0.1	16	11	0.58	5.1	6.4
	IPL	b.d.l.	b.d.l.	b.d.l.	14	3	b.d.l.	50	b.d.l.	b.d.l.	8	0.5	b.d.l.	25	b.d.l.	b.d.l.	1%	38%	0.02		
YG3	CL	22	2	1	29	2	0.3	20	0.3	b.d.l.	10	2	0.2	10	0.4	b.d.l.	7	1	0.84	3.5	6.4

	IPL	b.d.l.	3	0.4	26	3	b.d.l.	49	b.d.l.	b.d.l.	1	1	b.d.l.	16	b.d.l.	b.d.l.	1%	23%	0.21	
YG4	CL	25	2	0.5	31	2	0.3	20	0.3	0.1	9	1	0.1	8	0.3	0.1	13	3	0.83	3.1	6.2
	IPL	b.d.l.	3	1	19	5	b.d.l.	51	b.d.l.	b.d.l.	b.d.l.	3	b.d.l.	17	b.d.l.	b.d.l.	0%	27%	0.03	
YG5	CL	26	2	1	32	2	0.2	19	0.3	b.d.l.	9	1	0.2	7	0.4	b.d.l.	16	10	0.61	3.4	6.2
	IPL	b.d.l.	0.4	b.d.l.	29	b.d.l.	b.d.l.	43	b.d.l.	b.d.l.	5	b.d.l.	b.d.l.	22	b.d.l.	b.d.l.	0%	36%	0.03	
YG6	CL	23	3	0.7	27	3	0.4	19	0.4	0.1	10	2	0.4	9	1	0.1	4	1	0.8	4.4	6.4
	IPL	b.d.l.	b.d.l.	b.d.l.	b.d.l.	b.d.l.	b.d.l.	b.d.l.	b.d.l.	b.d.l.	b.d.l.	b.d.l.	b.d.l.	b.d.l.	b.d.l.	b.d.l.	b.d.l.	22%	n.d.		
YG7	CL	36	b.d.l.	b.d.l.	30	b.d.l.	b.d.l.	16	b.d.l.	b.d.l.	11	b.d.l.	b.d.l.	7	b.d.l.	b.d.l.	9	3	0.75	4.7	6.1
	IPL	b.d.l.	b.d.l.	b.d.l.	b.d.l.	b.d.l.	b.d.l.	b.d.l.	b.d.l.	b.d.l.	b.d.l.	b.d.l.	b.d.l.	b.d.l.	b.d.l.	b.d.l.	b.d.l.	20%	n.d.		
YG8	CL	24	3	1.1	26	4	1	20	1	0.1	9	2	1	7	0.5	0.1	19	8	0.67	5.3	6.3
	IPL	b.d.l.	b.d.l.	b.d.l.	b.d.l.	b.d.l.	b.d.l.	b.d.l.	b.d.l.	b.d.l.	b.d.l.	b.d.l.	b.d.l.	b.d.l.	b.d.l.	b.d.l.	b.d.l.	19%	n.d.		
YG9	CL	24	4	1.0	26	5	0.4	20	1	0.1	9	2	1	7	0.4	0.2	30	12	0.68	5	6.3
	IPL	b.d.l.	b.d.l.	b.d.l.	b.d.l.	b.d.l.	b.d.l.	b.d.l.	b.d.l.	b.d.l.	b.d.l.	b.d.l.	b.d.l.	b.d.l.	b.d.l.	b.d.l.	b.d.l.	12%	n.d.		
YO1	CL	32	2	b.d.l.	33	b.d.l.	b.d.l.	18	b.d.l.	b.d.l.	8	b.d.l.	b.d.l.	6	b.d.l.	b.d.l.	1	0.4	0.65	3.7	5.9
	IPL	b.d.l.	b.d.l.	b.d.l.	b.d.l.	b.d.l.	b.d.l.	b.d.l.	b.d.l.	b.d.l.	b.d.l.	b.d.l.	b.d.l.	b.d.l.	b.d.l.	b.d.l.	b.d.l.	12%	n.d.		
YO2	CL	16	b.d.l.	b.d.l.	19	b.d.l.	b.d.l.	34	b.d.l.	b.d.l.	9	b.d.l.	b.d.l.	21	b.d.l.	b.d.l.	0.2	0.4	0.35	4.4	6.6
	IPL	b.d.l.	b.d.l.	b.d.l.	b.d.l.	b.d.l.	b.d.l.	b.d.l.	b.d.l.	b.d.l.	b.d.l.	b.d.l.	b.d.l.	b.d.l.	b.d.l.	b.d.l.	b.d.l.	14%	n.d.		
YO3	CL	25	b.d.l.	b.d.l.	26	b.d.l.	b.d.l.	24	b.d.l.	b.d.l.	13	b.d.l.	b.d.l.	13	b.d.l.	b.d.l.	0.1	0.4	0.22	4	6.4
	IPL	b.d.l.	b.d.l.	b.d.l.	b.d.l.	b.d.l.	b.d.l.	b.d.l.	b.d.l.	b.d.l.	b.d.l.	b.d.l.	b.d.l.	b.d.l.	b.d.l.	b.d.l.	b.d.l.	10%	n.d.		
KS1	CL	35	b.d.l.	b.d.l.	37	b.d.l.	b.d.l.	17	b.d.l.	b.d.l.	6	b.d.l.	b.d.l.	5	b.d.l.	b.d.l.	0.4	0.09	0.84	2.7	5.7
	IPL	b.d.l.	b.d.l.	b.d.l.	b.d.l.	b.d.l.	b.d.l.	b.d.l.	b.d.l.	b.d.l.	b.d.l.	b.d.l.	b.d.l.	b.d.l.	b.d.l.	b.d.l.	b.d.l.	12%	n.d.		
KS2	CL	33	3	0.8	31	1	b.d.l.	16	b.d.l.	b.d.l.	8	2	b.d.l.	5	b.d.l.	b.d.l.	1	0.4	0.75	5.1	6.0
	IPL	b.d.l.	b.d.l.	b.d.l.	b.d.l.	b.d.l.	b.d.l.	b.d.l.	b.d.l.	b.d.l.	b.d.l.	b.d.l.	b.d.l.	b.d.l.	b.d.l.	b.d.l.	b.d.l.	11%	n.d.		
KS3	CL	32	3	1.3	30	3	b.d.l.	16	b.d.l.	b.d.l.	7	1	b.d.l.	6	b.d.l.	b.d.l.	1	1	0.47	5.1	6.0

	IPL	b.d.l.	b.d.l.	b.d.l.	b.d.l.	b.d.l.	b.d.l.	b.d.l.	b.d.l.	b.d.l.	b.d.l.	b.d.l.	b.d.l.	b.d.l.	b.d.l.	b.d.l.	b.d.l.	24%	n.d.		
KS4	CL	31	b.d.l.	b.d.l.	35	b.d.l.	b.d.l.	18	b.d.l.	b.d.l.	10	b.d.l.	b.d.l.	6	b.d.l.	b.d.l.	0.1	0.1	0.53	2.4	6.0
	IPL	b.d.l.	b.d.l.	b.d.l.	b.d.l.	b.d.l.	b.d.l.	b.d.l.	b.d.l.	b.d.l.	b.d.l.	b.d.l.	b.d.l.	b.d.l.	b.d.l.	b.d.l.	b.d.l.	14%	n.d.		
KB1	CL	20	2	0.5	31	2	0.4	29	1	0.1	7	1	0.1	5	0.4	0.04	29	1	0.97	2.4	6.0
	IPL	b.d.l.	b.d.l.	b.d.l.	b.d.l.	b.d.l.	b.d.l.	b.d.l.	b.d.l.	b.d.l.	b.d.l.	b.d.l.	b.d.l.	b.d.l.	b.d.l.	b.d.l.	b.d.l.	60%	n.d.		
KB2	CL	20	2	0.5	31	2	0.5	30	0.4	0.1	6	1	0.1	6	0.2	0.1	28	1	0.97	2.3	5.9
	IPL	b.d.l.	12	b.d.l.	15	b.d.l.	b.d.l.	51	6	b.d.l.	2	b.d.l.	b.d.l.	9	5	b.d.l.	2%	39%	0.44		
KB3	CL	19	2	1	28	2	1	30	1	0.2	7	1	0.2	8	0.5	0.1	30	1	0.95	3.1	6.1
	IPL	b.d.l.	8	b.d.l.	b.d.l.	b.d.l.	b.d.l.	60	5	b.d.l.	3	b.d.l.	b.d.l.	18	6	b.d.l.	1%	37%	0.15		
KB4	CL	17	2	0.3	33	2	0.3	32	0.5	0.1	7	1	0.1	6	0.3	0.1	49	2	0.97	1.1	5.9
	IPL	b.d.l.	b.d.l.	b.d.l.	b.d.l.	b.d.l.	b.d.l.	73	1	b.d.l.	b.d.l.	1	1	21	2	0.3	0%	38%	n.d.		
KG1	CL	23	4	1	26	4	0.5	22	1	0.3	7	2	1	6	0.5	0.2	21	7	0.71	5.2	6.2
	IPL	b.d.l.	b.d.l.	b.d.l.	b.d.l.	b.d.l.	b.d.l.	b.d.l.	b.d.l.	b.d.l.	b.d.l.	b.d.l.	b.d.l.	b.d.l.	b.d.l.	b.d.l.	b.d.l.	18%	n.d.		
KG2	CL	22	3	1	26	5	1	24	1	0.3	8	2	1	6	1	0.2	21	8	0.71	4.8	6.2
	IPL	b.d.l.	b.d.l.	b.d.l.	b.d.l.	b.d.l.	b.d.l.	b.d.l.	b.d.l.	b.d.l.	b.d.l.	b.d.l.	b.d.l.	b.d.l.	b.d.l.	b.d.l.	b.d.l.	18%	n.d.		
OO1	CL	27	3	1.2	28	3	1	19	1	b.d.l.	7	1	0.3	8	1	b.d.l.	5	2	0.67	4.8	6.2
	IPL	b.d.l.	b.d.l.	b.d.l.	b.d.l.	b.d.l.	b.d.l.	b.d.l.	b.d.l.	b.d.l.	b.d.l.	b.d.l.	b.d.l.	b.d.l.	b.d.l.	b.d.l.	b.d.l.	32%	n.d.		
OO2	CL	31	2	b.d.l.	32	2	b.d.l.	19	b.d.l.	b.d.l.	7	1	b.d.l.	7	b.d.l.	b.d.l.	1	0.3	0.73	3.9	6.0
	IPL	b.d.l.	b.d.l.	b.d.l.	b.d.l.	b.d.l.	b.d.l.	b.d.l.	b.d.l.	b.d.l.	b.d.l.	b.d.l.	b.d.l.	b.d.l.	b.d.l.	b.d.l.	b.d.l.	19%	n.d.		

1149

Table 5. Summarizes the fractional abundances of the brGDGT compounds of the core lipid (CL) and intact polar lipid (IPL) fractions in the sediments. The amounts of CL brGDGTs and crenarchaeol at each station are reported normalized per gram TOC, while the IPL abundances are expressed as the percentage of IPLs relative to the total amount of brGDGTs per site. The calculated BIT index for the IPL and CL fractions [Eq. 2] and the reconstructed MAT [Eq. 5] and pH [Eq. 3 and 4] for the CL fraction are reported. B.d.l. indicates that the amounts measured were below detection limit.

Sample	Fraction	Ia	Ib	Ic	IIa	IIb	IIc	IIIa	IIIb	IIIc	IIa'	IIb'	IIc'	IIIa'	IIIb'	IIIc'	Σ brGDGTs (µg. g TOC^{-1}) IPL (%)	crenarchaeol (µg. g TOC^{-1}) IPL (%)	BIT	MAT (°C)	pH
YM2	CL	14	2	1	18	2	0.5	16	1	0.2	13	4	0.3	26	2	0.5	87	1.3	0.98	5.4	7.1
	IPL	11	3	1	13	3	1	15	1	0.2	15	7	0.3	27	3	0.2	6%	54%	0.75		
YM3	CL	16	2	0.4	22	2	0.3	20	0.5	0.1	13	3	0.1	19	1	0.1	82	1.0	0.99	4.2	6.8
	IPL	11	3	2	20	3	1	17	1	0.3	13	3	0.3	22	3	0.1	7%	45%	0.85		
YM4	CL	14	3	1	22	3	0.4	22	1	0.1	13	3	0.2	18	1	0.2	36	0.2	0.99	4.3	6.8
	IPL	b.d.l.	b.d.l.	b.d.l.	b.d.l.	b.d.l.	b.d.l.	b.d.l.	b.d.l.	b.d.l.	b.d.l.	b.d.l.	b.d.l.	b.d.l.	b.d.l.	b.d.l.	b.d.l.	30%	n.d.		
YG1	CL	20	3	1	24	3	0.4	20	1	0.1	12	2	0.3	13	1	0.1	18	2.6	0.86	4.5	6.6
	IPL	20	4	1	20	8	1	22	1	0.1	9	2	2	9	1	b.d.l.	2%	18%	0.37		
YG2	CL	30	3	1	25	2	0.3	11	0	0.1	15	2	0	10	1	0.1	12	2.5	0.81	6.4	6.6
	IPL	27	4	1	19	7	1	18	1	b.d.l.	10	2	1	10	1	b.d.l.	5%	9%	0.71		
YG3	CL	23	3	1	25	3	0.4	18	1	0.1	12	2	0	11	1	0.2	15	3.1	0.81	5	6.5
	IPL	19	3	1	17	8	1	23	1	0.3	12	3	2	10	1	0.1	5%	20%	0.47		
YG7	CL	22	3	1	25	3	0.4	18	1	0.1	13	2	0.3	12	1	0.1	28	3.8	0.87	4.7	6.6
	IPL	23	3	1	25	5	0.5	20	1	b.d.l.	4	6	1	10	1	b.d.l.	4%	26%	0.42		
YG8	CL	20	3	1	25	5	0.4	23	1	0.1	9	2	1	8	1	0.2	69	20	0.75	4.7	6.4
	IPL	19	3	1	21	7	1	26	1	0.4	7	3	2	8	1	b.d.l.	6%	13%	0.55		

YG9	CL	21	3	1	25	5	0.4	22	1	0.1	9	2	1	10	1	0.2	62	19	0.74	4.7	6.4
	IPL	17	5	1	20	6	1	17	2	b.d.l.	7	5	2	15	2	b.d.l.	12%	45%	0.31		
YO1	CL	29	4	1	21	5	1	15	1	0.1	9	3	1	8	1	0.3	12	11	0.47	7.6	6.5
	IPL	33	4	1	13	7	1	14	1	0.2	8	4	2	9	2	0.2	8%	15%	0.28		
YO2	CL	35	4	1	21	3	0.4	10	1	0.2	10	4	1	8	1	0.3	16	14	0.49	8.6	6.5
	IPL	24	2	0.1	5	b.d.l.	0.5	20	1	b.d.l.	14	17	3	11	2	b.d.l.	4%	25%	0.10		
YO3	CL	33	4	1	18	2	0.5	11	1	0.2	10	7	2	9	2	0.4	12	12.8	0.43	9.2	6.7
	IPL	30	4	1	12	8	1	12	1	0.4	11	5	3	8	2	1	12%	20%	0.27		
KS1	CL	39	3	1	22	3	0.2	9	0.4	0.1	10	2	1	8	1	0.2	19	20	0.46	8.8	6.4
	IPL	32	3	0.2	17	10	1	11	2	0.5	9	1	4	7	3	0.5	8%	22%	0.19		
KS2	CL	42	2	1	23	2	0.2	8	0.2	0.03	9	1	0.3	11	0.4	0.1	11	16	0.39	8.5	6.3
	IPL	39	2	1	22	2	0.3	8	1	b.d.l.	10	2	1	11	1	b.d.l.	8%	22%	0.16		
KS3	CL	40	4	1	23	3	0.3	9	1	0.1	8	3	1	6	1	0.2	8.3	8.2	0.46	8.7	6.2
	IPL	32	1	1	11	7	0.3	17	1	0.5	18	0	2	7	2	0.4	6%	12%	0.30		
KS4	CL	31	5	1	17	6	1	9	1	0.1	9	5	2	11	2	0.6	3.9	33	0.08	9.5	6.7
	IPL	42	3	1	11	7	0.4	7	1	0.5	8	6	3	8	2	0.5	14%	14%	0.09		
KB1	CL	19	2	0.3	34	1	0.3	31	0.3	0.1	7	1	0.1	5	0	0.02	83	0.7	0.99	1.3	5.9
	IPL	16	2	0.4	37	2	1	30	0.3	b.d.l.	6	0.5	0.1	6	0	b.d.l.	11%	53%	0.92		
KB2	CL	19	2	0.3	33	1	0.3	33	0.5	0.1	5	1	0.1	5	0	0.04	53	0.3	0.99	1.5	5.7
	IPL	17	2	1	33	2	1	30	0.4	b.d.l.	7	1	b.d.l.	5	0	b.d.l.	11%	53%	0.95		
KB3	CL	20	2	1	28	2	1	32	1	1	5	1	0.1	6	1	0.1	56	1.0	0.98	3.4	5.9
	IPL	17	3	1	28	3	1	31	1	1	7	1	0.1	6	1	0.03	10%	44%	0.88		
KB4	CL	14	1	0.3	29	1	0.3	40	1	0.2	6	1	0.1	6	0	0.1	82	1.0	0.99	1.6	5.9
	IPL	12	2	0.4	33	2	1	37	0.5	0.1	3	0.3	0.1	8	b.d.l.	b.d.l.	5%	40%	0.86		

KG1	CL	19	3	1	27	4	0.4	27	1	0.2	7	2	1	7	1	0.2	56	12	0.81	3.9	6.2
	IPL	17	2	1	24	4	0.4	32	1	b.d.l.	9	1	2	8	1	b.d.l.	4%	11%	0.58		
KG2	CL	20	3	1	25	4	1	27	2	0.4	7	2	1	8	1	0.1	61	11	0.83	4.3	6.2
	IPL	17	4	2	16	6	1	28	3	1	10	3	3	8	1	b.d.l.	4%	25%	0.37		
OO1	CL	28	3	1	25	5	1	18	1	0.2	8	2	1	7	1	0.2	32	16	0.64	5.9	6.3
	IPL	29	4	1	20	8	1	16	1	b.d.l.	7	3	1	6	1	0.1	7%	19%	0.34		
OO2	CL	27	3	1	25	4	0.5	18	1	0.2	8	2	1	7	1	0.2	35	23	0.57	5.8	6.3
	IPL	26	4	1	23	6	1	20	1	0.1	7	2	1	7	1	0.2	11%	21%	0.38		

1154

Table 6. Summarizes the fractional abundances of the brGDGT compounds of the watershed soils and the coastal cliffs. The amounts of CL and IPL brGDGTs and crenarchaeol at each station are reported. The calculated BIT index [Eq. 2] is reported for the CL and IPL fraction, and the reconstructed MAT [Eq. 5] and pH [Eq. 3 and 4] are reported for the CL fraction. B.d.l. indicates that the amounts measured were below detection limit.

Sample	Ia	Ib	Ic	IIa	IIb	IIc	IIIa	IIIb	IIIc	IIa'	IIb'	IIc'	IIIa'	IIIb'	IIIc'	Σ brGDGTs (µg. g OC^{-1})	crenarchaeol (µg. g OC^{-1})	BIT	MAT (°C)	pH
S_1	8	3	0.2	18	2	0.2	27	0.4	0.1	15	4	0.3	20	1	0.3	n.d.	n.d.	1.00	4	7.0
S_2	65	1	0.4	29	0.4	0.2	3	b.d.l.	b.d.l.	0.5	0.1	b.d.l.	0.3	b.d.l.	b.d.l.	86	0.003	1.00	10	4.1
CC_YM1	25	4	1	21	3	1	23	2	1	7	2	0.3	9	1	0.1	45	8	0.83	7	6.3
CC_YM2	14	5	1	24	3	0.2	30	0.5	0.1	10	2	0.1	10	0.5	0.1	13	0.2	0.98	4	6.5
CC_YM3	28	5	2	21	3	1	20	1	1	8	2	0.2	8	1	0.1	43	9	0.81	8	6.4
CC_YM4	15	4	1	23	3	0.4	28	0.4	0.1	13	2	0.2	10	0.4	0.1	51	2	0.97	4	6.4
CC_YM5	24	0.2	b.d.l.	42	1	0.5	32	0.0	b.d.l.	b.d.l.	b.d.l.	b.d.l.	0	b.d.l.	b.d.l.	n.d.	n.d.	1.00	-1	3.2
CC_YM6	8	3	0.3	27	2	b.d.l.	40	0.2	b.d.l.	8	0	b.d.l.	11	0.3	0.1	22	0.04	1.00	2	6.4
CC_YM7	17	4	1	25	3	0.4	25	0.5	0.1	12	3	0.2	9	0.5	0.1	n.d.	n.d.	0.95	4	6.3
CC_YM8	23	4	1	25	3	0.5	22	1	0.2	10	2	0.2	8	0.5	0.1	23	2	0.91	5	6.5
CC_YM9	17	5	1	26	3	0.4	25	0.5	0.1	11	3	0.2	9	0.4	0.1	21	0.8	0.96	4	6.2
CC_YG1	29	4	1	25	3	0.3	13	0.4	0.1	12	2	0.5	9	0.5	0.1	32	11	0.71	6	6.4
CC_YG2	16	3	b.d.l.	30	2	b.d.l.	31	0.2	b.d.l.	10	2	b.d.l.	7	0.3	b.d.l.	7.6	0.02	0.99	2	4.9
CC_YG3	16	5	1	25	4	b.d.l.	22	1	0.2	12	3	b.d.l.	10	1	0.2	18	0.8	0.95	4	6.6

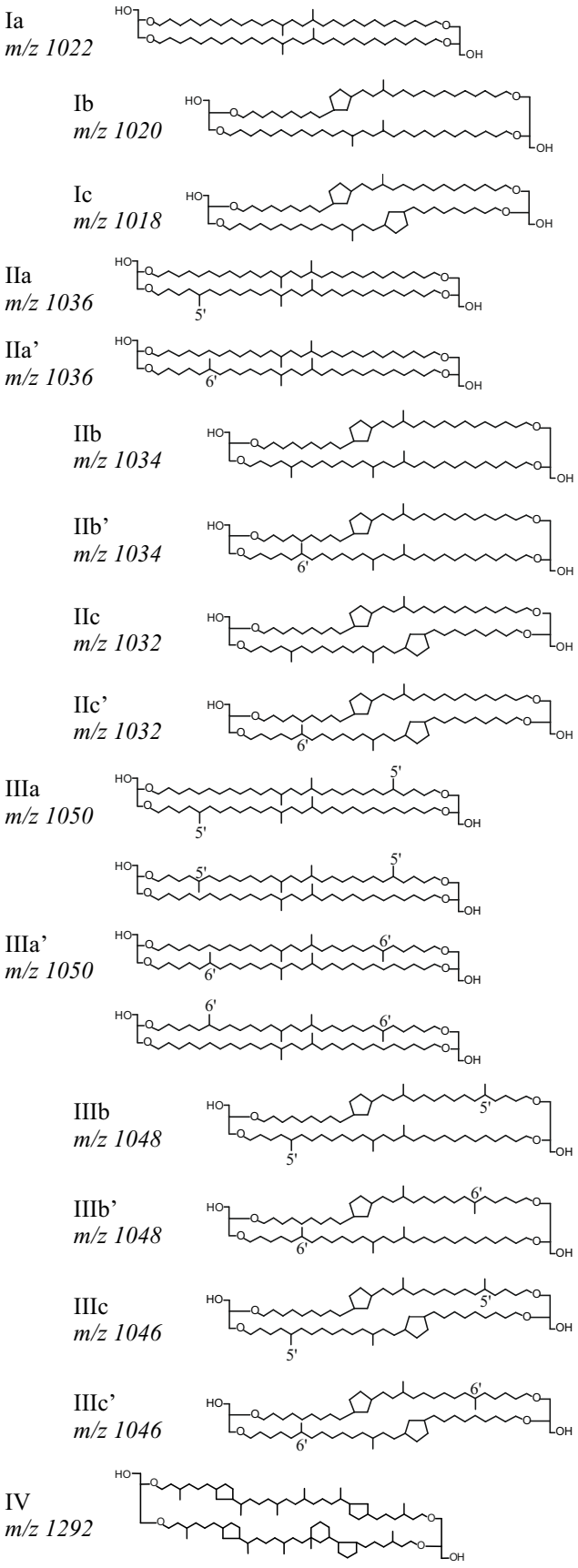

Fig. 1. Chemical structures of branched GDGTs (I-III) and crenarchaeol (IV). The chemical structures of the hexa- and pentamethylated brGDGTs with cyclopentyl moiety(ies) IIb', IIc', IIIb' and IIIc' are tentatively assigned.

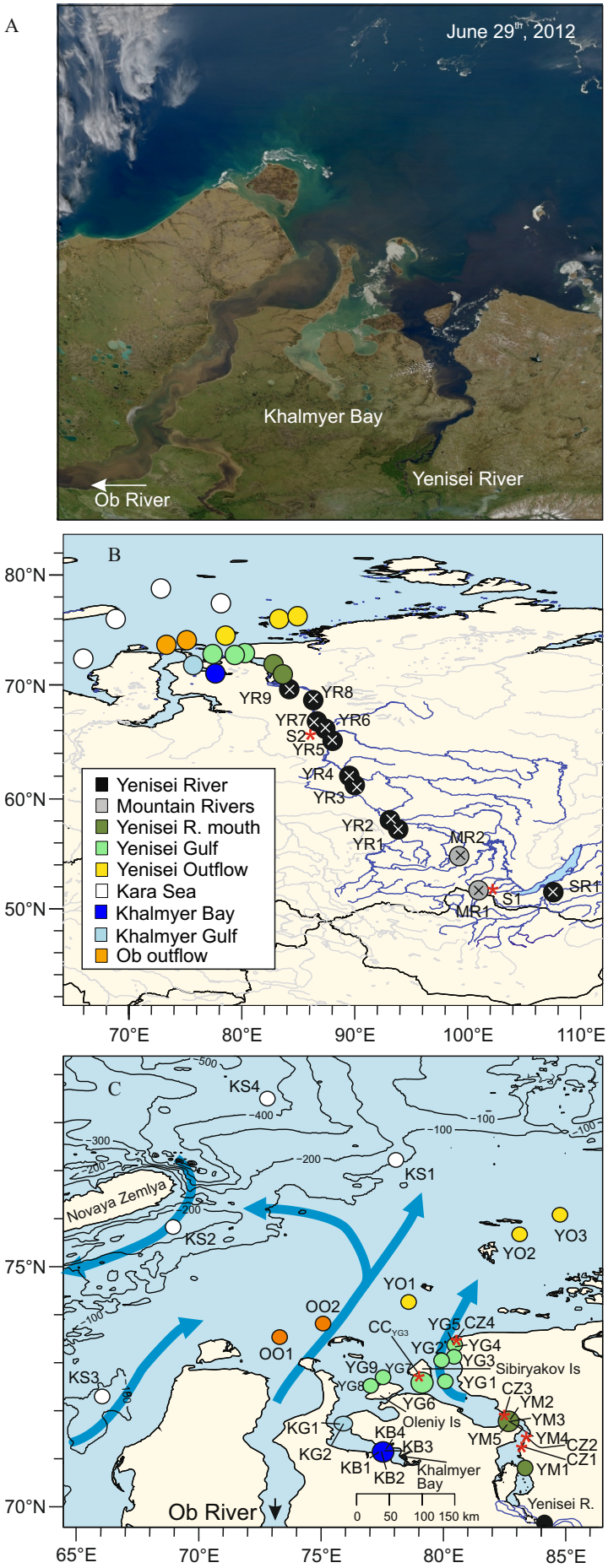

Fig. 2. A) Satellite image of the Ob River Mouth, the Khalmyer Bay and Yenisei River Mouth, showing the increase in sediment load in the Khalmyer Bay and Yenisei Gulf that can be related to coastal cliff erosion. NASA image courtesy Norman Kuring, Ocean Color Web. B) Overview map of the Yenisei River, with sample sites indicated. Red asterisks indicate sites of watershed soil samples. C) Map of the Kara Sea, with sampling locations and Yenisei and Ob River Mouths and Khalmyer Bay indicated. Asterisks indicate sampling sites of coastal cliff samples. In panel B) and C) symbol colours divide the stations in geographical zones, as reflected by the legend.

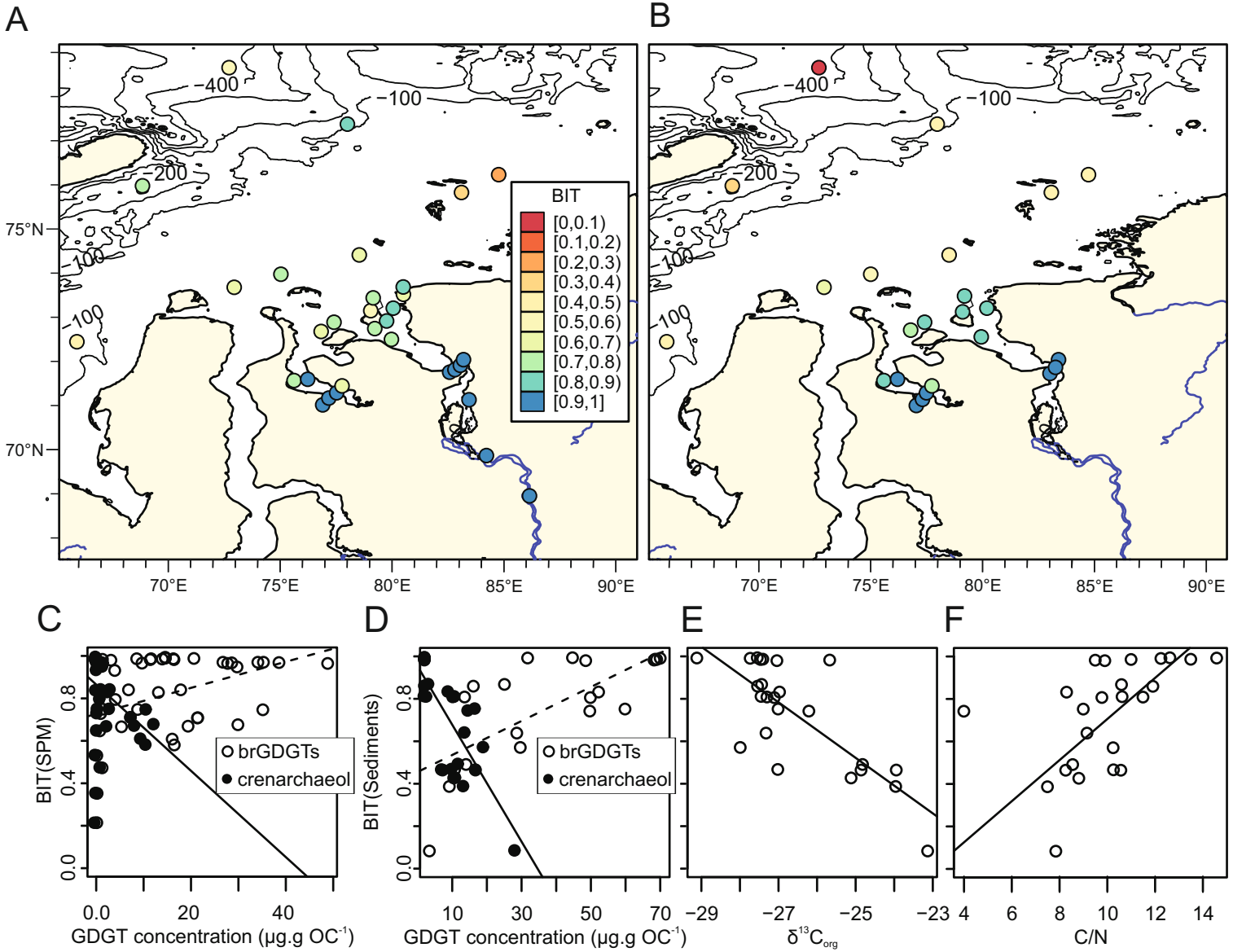

Fig. 3. A-B) Core lipid BIT values in suspended particulate matter (SPM; A) and sediments (B). Colours of the dots refer to the BIT-colour scale indicated. C-D) BIT values plotted vs. GDGT concentration, with brGDGTs plotted as closed symbols and crenarchaeol as open symbols, in both the SPM (C panel) and sediments (D panel). E-F) Sedimentary BIT-values plotted versus the sedimentary $\delta^{13}C_{org}$ values (E) and C/N ratio (F).

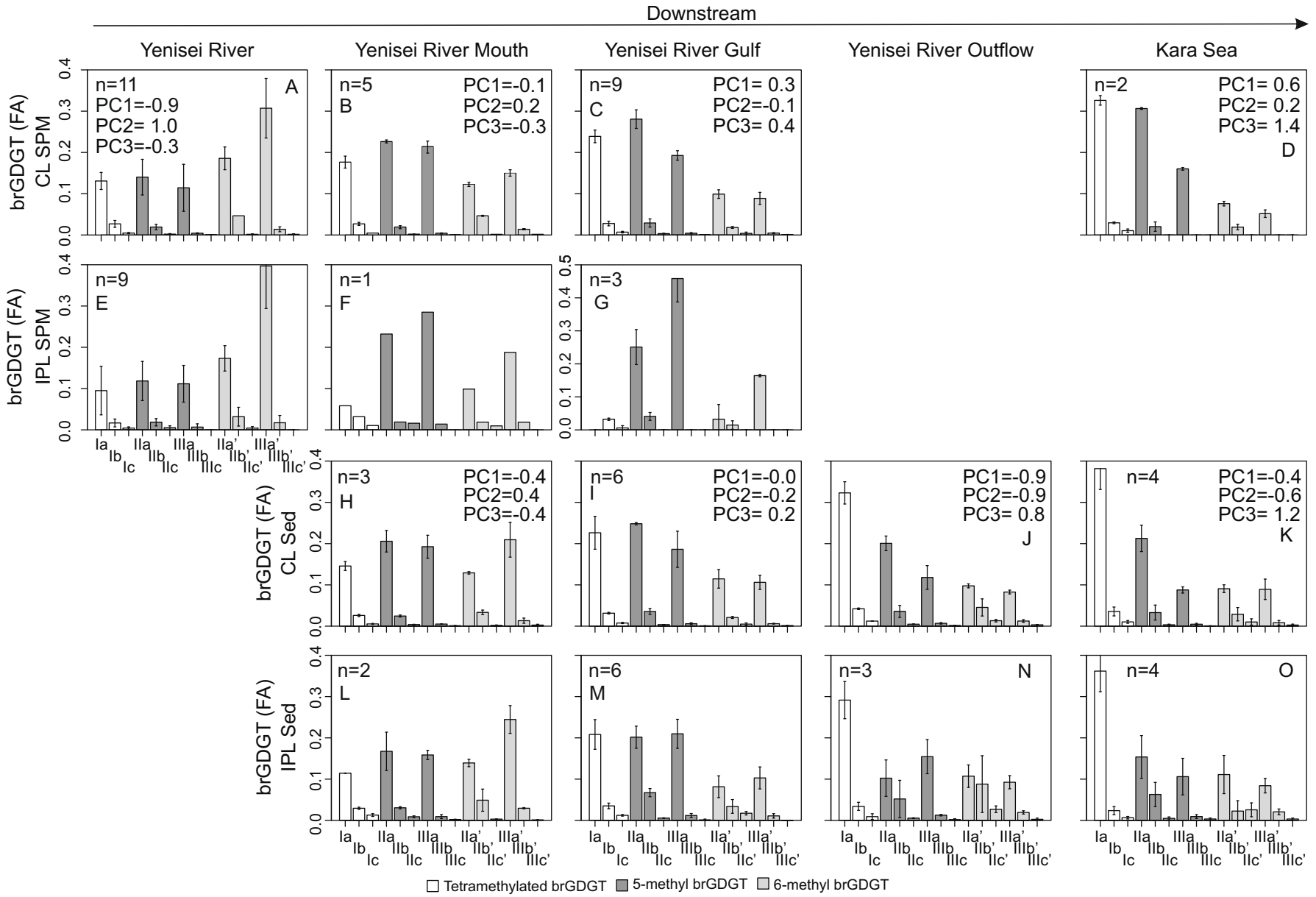

Fig. 4. Bar plots of the fractional abundance of brGDGTs in the CL (A-D and H-K) and IPL (E-G and L-O) fractions of the SPM (A-G) and sediments (H-O), respectively. The fractional abundances are averaged per geographical zone, as defined in Table 1. For the CL fraction, the average score on the first three PC is reported per geographical zone. For clarity, brGDGTs with a large standard deviation (sd) of their fractional abundance (reflecting the variance within the geographical zone) only have the lower halve of the range (range = 2 x sd) plotted. The colour of the bars refer to the brGDGT structure, as reflected in the figure legend. As only samples with >8 brGDGTs quantified were plotted, the number of observations per zone is reported, and zones without any samples with >8 compounds, have no corresponding bar plot.

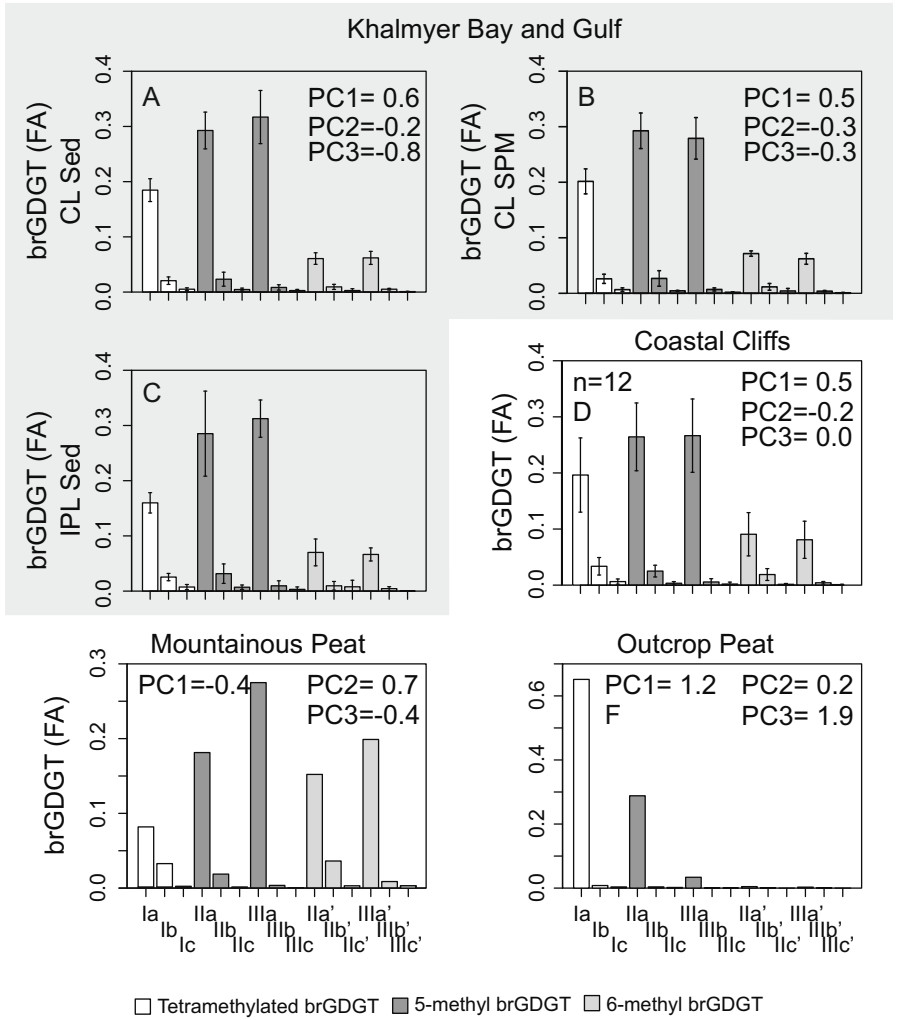

Fig. 5. Bar plots of the fractional abundance of brGDGTs in the CL (A, B, D) and IPL (C) fractions of the Khalmyer Bay and Gulf sediments (A, C) and SPM (B). Furthermore, a number of possible sources of brGDGTs is reported, being the coastal cliffs (D), a mountainous peat sample from the floodplain of a lake (E) and a lowland peat sampled at 2m depth (F). The fractional abundances are averaged for the Khalmyer Bay and Gulf (as defined in Table 1) combined. The number of observations per zone is reported, and to capture the variace between the samples in each dataset, the range indicated with the whiskers equals 2 x standard deviation. For the CL fraction, the average score on the first three PC is reported. The colour of the bars refer to the brGDGT structure, as reflected in the figure legend.

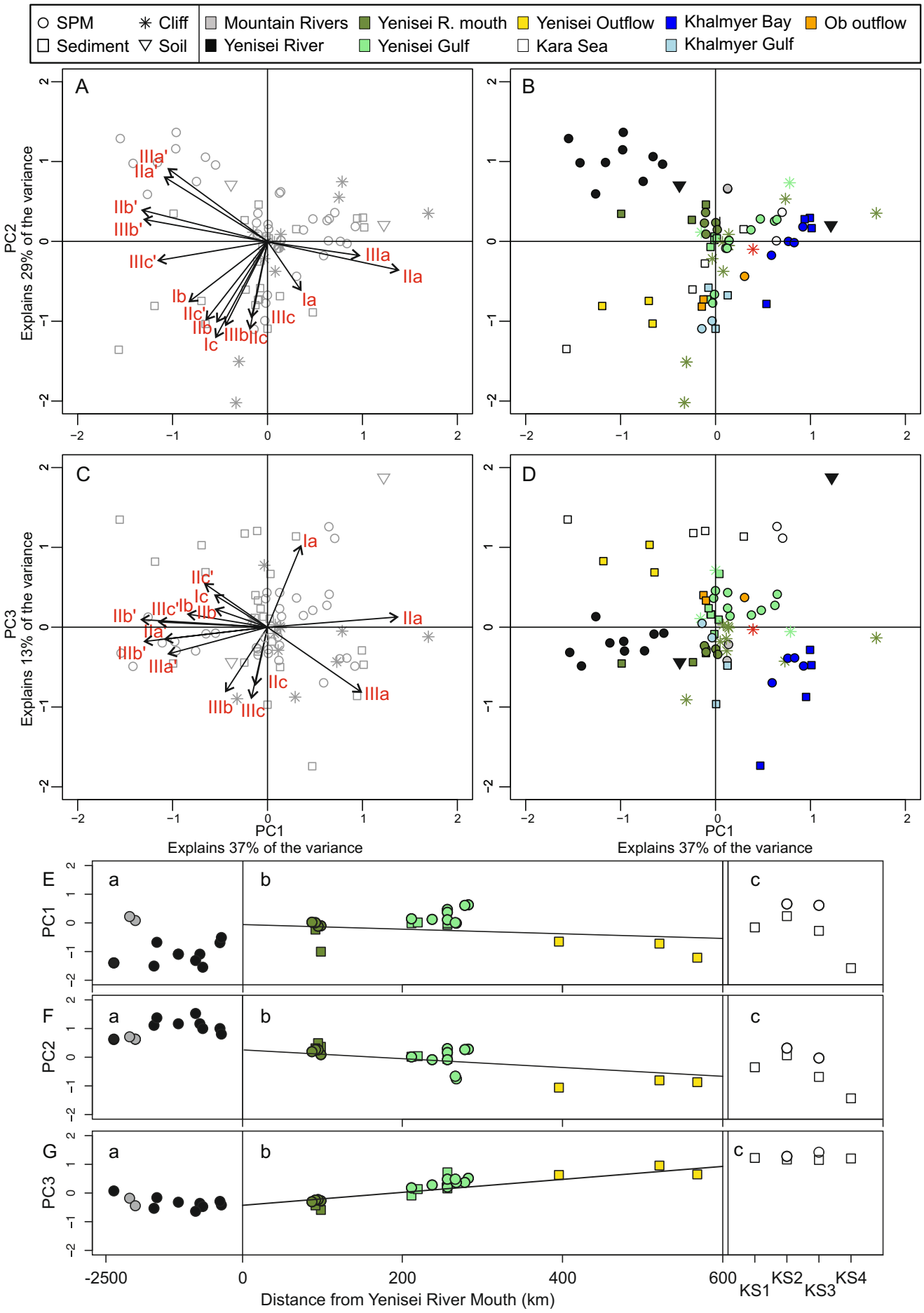

Fig. 6. Biplots of the principal components (PC) based on the fractional abundance of CL brGDGTs, for those samples that have more than 8 (out of 15) brGDGTs quantified. The first two (A, B) and first and third PC (C, D) are plotted, representing respectively 37, 29 and 13% of the variance. The loadings of the variables (A, C) and the scores of the sites (B, D) are plotted. The score of each station is calculated using the relative abundance of each compound per station and its loading on the PC. Round symbols indicate SPM brGDGT distributions, rectangles indicate sedimentary brGDGT distributions, asterisks indicate coastal cliff samples and triangles indicate watershed soil samples. The colour of the symbols reflects the geographical zone of the station. The red coloured asterisk gives the score of the weighed average of the coastal cliff brGDGT distributions (n=12). E-G) Plots of the score on the PC1-3. In subplots a and b the scores are plotted against the straight distance from the river Mouth (83°17.0383 N, 70°99.675 E), where subplot a has a different scale compared to subplot b. The 4 Kara Sea samples are plotted in subplot c, as the distance from the river Mouth will be a poor comparison for the length of the flowpath for these samples.

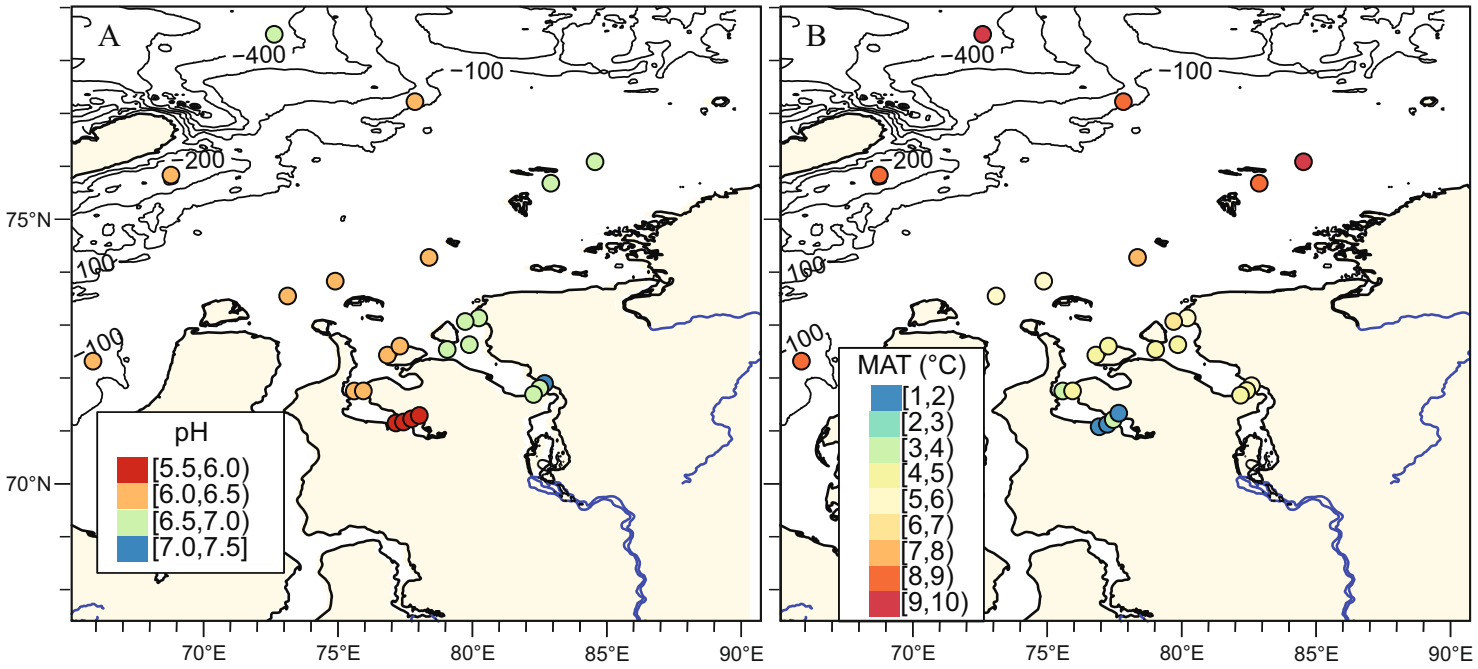

Fig. 7. A) Reconstructed pH [Eq. 3 and 4] and B) reconstructed MAT [Eq. 5], based on the brGDGT distribution in surface sediments.